

Record Ages of non-Markovian Scale-Invariant Random Walks

Léo Régnier,¹ Maxim Dolgushev,¹ and Olivier Bénichou^{1,*}

¹*Laboratoire de Physique Théorique de la Matière Condensée,
CNRS/Sorbonne Université, 4 Place Jussieu, 75005 Paris, France*

ABSTRACT

How long is needed for an observable to exceed its previous highest value and establish a new record? This time, known as the age of a record plays a crucial role in quantifying record statistics. Until now, general methods for determining record age statistics have been limited to observations of either independent random variables or successive positions of a Markovian (memoryless) random walk. Here we develop a theoretical framework to determine record age statistics in the presence of memory effects for continuous non-smooth processes that are asymptotically scale-invariant. Our theoretical predictions are confirmed by numerical simulations and experimental realizations of diverse representative non-Markovian random walk models and real time series with memory effects, in fields as diverse as genomics, climatology, hydrology, geology and computer science. Our results reveal the crucial role of the number of records already achieved in time series and change our view on analysing record statistics.

INTRODUCTION

The statistics of records in a discrete time series $(X_t)_{t=0,1,\dots}$ is one of the main topics of interest in the study of extreme events [1], with applications in an increasing number of fields. A record event occurs at time t if all prior observations $(X_{t'})_{t'=0,\dots,t-1}$ are smaller than the last value X_t . In this context, the inter record times τ_n , also called record ages [2–9], between the n^{th} and $(n+1)^{\text{st}}$ record, are pivotal, as they characterize the time of occurrence of the next record breaking event such as heatwaves [10], earthquakes [11, 12] or record temperatures [13].

The theory of records has been studied since the mid-20th century [14, 15], and is well understood when the random variables $(X_t)_{t=0,1,\dots}$ are independent and identically distributed (i.i.d.) [16–18]. An important step in the study of records was recently made when observations are the successive positions of a Markovian RW [4, 19–22], $X_{t+1} = X_t + \eta_{t+1}$, where the steps $(\eta_t)_{t=0,1,\dots}$ are still i.i.d. and symmetric. In this situation, record ages are strictly given by the time T needed to reach a given value for the first time, regardless of the past. This time follows an algebraic tail distribution $\mathbb{P}(T \geq \tau) \propto \tau^{-\theta}$, where θ is the persistence exponent [23], provided by the celebrated Sparre-Andersen theorem [24], yielding $\theta = 1/2$. We emphasize that, despite the fact that this RW model accounts for correlations between the observations $(X_t)_{t=0,1,\dots}$, the steps $(\eta_t)_{t=0,1,\dots}$ themselves are independent. As a result, this model cannot account for memory effects in the increments.

However, as a general rule, real time series are not only correlated but also exhibit such memory effects. When the evolution of an observable is influenced by interactions with hidden degrees of freedom, such as the previ-

ous steps of the RW or its interaction with the environment, it cannot be modeled as a Markov process.

This is typically the case for displacement data from various tracers (microspheres, polymers, cells, vacuoles...) in simple [25] and viscoelastic fluids [26–28], soil [29, 30] and air temperatures [31], river flows [32, 33], nucleotide sequence locations [34, 35] and Ethernet traffic [36–38]. So far, as highlighted in the recent review [4], almost nothing is known about the record age statistics of non-Markovian processes. The only exceptions concern processes amenable to a Markovian process by adding an extra degree of freedom [3, 8, 39], and a numerical observation in the specific case of the fractional Brownian motion [9]. Here, we provide a general scaling theory which determines the time dependence of the record age statistics of non-Markovian RWs. We show that memory effects significantly alter these statistics. They are no longer solely governed by the persistence exponent θ , but also by another explicitly calculated exponent, which is the hallmark of non-Markovian dynamics.

RESULTS

A. Main Results

We consider a general non-Markovian symmetric RW, whose successive positions form a time series $(X_t)_{t=0,1,\dots}$. These positions satisfy $X_{t+1} = X_t + \eta_{t+1}$, where now the statistics of the steps $(\eta_t)_{t=0,1,\dots}$ may exhibit (I) long-range correlations, (II) interactions with the environment (e.g. footprints left along the trajectory), or (III) explicit space-time dependence (see Fig. 1). Essentially all statistical mechanisms that lead to non-Markovian evolution are encompassed by these features of X_t [40]. In turn, they allow to account for a variety of real time series displaying memory effects [41, 42]. At large time, X_t is assumed to converge to a scale-invariant process that is continuous (i.e., excluding broadly dis-

* benichou@lptmc.jussieu.fr

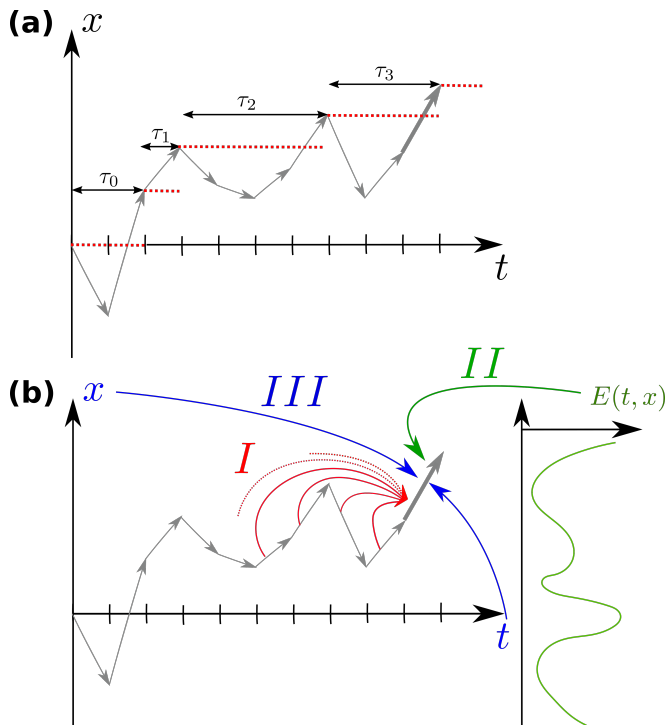


FIG. 1. **Record ages for non-Markovian random walks (RWs).** (a) Sketch of a space time trajectory of the RW represented by successive discrete steps η_t (grey arrows). The records in the trajectory are identified by red dotted lines. The record age τ_n of the RW is defined as the time between the n^{th} and $(n+1)^{\text{st}}$ records. (b) Different statistical mechanisms giving rise to a non-Markovian evolution: The statistics of the RW steps η_t may depend on (I) the previous steps of the walk (red arrow), (II) the environment with which the RW interacts (green arrow, schematically represented by the function $E(t, x)$), or (III) the current time or position (blue arrows). In this article, we show that these memory effects strongly modify the record age statistics, which are no longer simply given by the usual persistence exponent θ , but also by a distinct exponent that we determine explicitly.

tributed steps η_t) and non-smooth [23] (meaning that, as for the standard Brownian motion, the trajectory is irregular, having at each point an infinite derivative). Under these conditions, the process is characterized by a walk dimension [40] $d_w > 1$, such that $X_t \propto t^{1/d_w}$, and the random variable $X_t/t^{1/d_w}$ is asymptotically independent of t . To account for potential aging in the increments, X_t is more generally assumed to have scale-invariant increments, meaning that, for $1 \ll t \ll T$, $X_{t+T} - X_T \propto t^{1/d_w^0} T^{\alpha/2}$. This defines the aging exponent α [43, 44] ($\alpha > 0$ corresponding qualitatively to accelerating processes and $\alpha < 0$ to slowing down processes) and an effective walk dimension at short times $d_w^0 \equiv (d_w^{-1} - \alpha/2)^{-1}$. We stress that the class of processes that we consider here covers a very broad range of examples of non-Markovian RWs, as detailed below, despite not covering the particular cases of Lévy flights [19] (which are discontinuous) or of the Random Acceleration

Process [3] (smooth), which would require a different approach.

We report that the tail distribution $S(n, \tau) \equiv \mathbb{P}(\tau_n \geq \tau)$ of the record age τ_n asymptotically obeys a scaling behaviour $S(n, \tau) = n^{-1} \psi(\tau/n^{d_w})$, displaying two universal distinct algebraic regimes :

$$S(n, \tau) \propto \begin{cases} \frac{1}{n} \left(\frac{n^{d_w}}{\tau} \right)^{\frac{1}{d_w^0}} & \text{for } n^{d_w - d_w^0} \ll \tau \ll n^{d_w}, \\ \frac{1}{n} \left(\frac{n^{d_w}}{\tau} \right)^{\theta} & \text{for } 1 \ll n^{d_w} \ll \tau, \end{cases} \quad (1)$$

where ψ is a process dependent scaling function and the persistence exponent θ has been defined above. Equation (1) explicitly determines the n and τ dependence of the record age statistics of non-Markovian RWs. Fundamental consequences of our results include: (i) In regime 1, defined by $n^{d_w - d_w^0} \ll \tau \ll n^{d_w}$, the record time's decay is governed by an exponent different from θ . While it is not unexpected that the memory of the past affects record age statistics for a non-Markovian process (in particular, it is known that it can change the persistence exponent [47, 64]), it is striking that the corresponding exponent is fully explicit and depends only on the effective walk dimension d_w^0 of the increments. Note that regime 1 can span several orders of magnitude as soon as sufficiently many records have been broken, and thus dominate the observations. (ii) In regime 2, defined by $\tau \gg n^{d_w}$, the decay in the record time can be very different from that of regime 1. This is particularly striking for processes with stationary increments for which the exponent involved in regime 2, $\theta = 1 - 1/d_w$ [44], is markedly different from the exponent $1/d_w^0 = 1/d_w$ of regime 1 (with the exception of Markovian RWs for which the two exponents are both $1/2$ and a single regime is recovered; note that this single regime of exponent $1/2$ is also obtained in the case of Lévy flights, which are not covered by our approach). (iii) The record age distribution ages, in the sense that it depends on the number n of records already achieved. Consequently, the observations of early record ages are not representative of later records and call for a careful analysis of real data (note that the record distribution also ages in time series with i.i.d. observations X_t , which are thus not of the form $X_{t+1} = X_t + \eta_{t+1}$ considered here, but the dependence of this distribution on the number of records and the corresponding statistical mechanisms are very different [4]). Finally, note that despite the existence of two regimes for record ages, because of the explicit dependence of the prefactors of $S(n, \tau)$ on n , the number of records at time t displays a single time regime $n \propto t^{1/d_w}$ (see Supplementary Information, SI).

B. Derivation of the results

The following outlines the derivation of these results (see SI Sec. S1 for details):

The first step consists in noting that, due to the scale-invariance of the process X_t , the time T_n to reach the n^{th} record, $T_n \equiv \sum_{k=0}^{n-1} \tau_k$, satisfies $T_n \propto n^{d_w}$ and its increments obey $T_{m+n} - T_m \propto m^{d_w - d_w^0} n^{d_w^0}$ (see SI Sec. S1.B). In other words, $\mathbb{P}(T_{m+n} - T_m \leq T)$ is a function of a single variable $T/(m^{d_w - d_w^0} n^{d_w^0})$. Then, $T_{m+n} - T_m = \sum_{k=m}^{m+n-1} \tau_k$ is dominated by the largest record age [40, 45] under the self-consistent assumption that $S(n, \tau) \propto n^{-1+\epsilon_1} \tau^{-y_1}$ for $\tau \ll n^{d_w}$ (regime 1) and $S(n, \tau) \propto n^{-1+\epsilon_2} \tau^{-y_2}$ for $\tau \gg n^{d_w}$ (regime 2) with y_i between 0 and 1. This results in the equation

$$\mathbb{P}(T_{m+n} - T_m \leq T) \simeq \mathbb{P}(\max(\tau_m, \dots, \tau_{m+n-1}) \leq T). \quad (2)$$

Adapting the argument of Ref. [46], we show for continuous scale-invariant non-smooth processes analytically (see Sec. S1.D of SI) and verify numerically (see Sec. S2.C of SI) that, in Eq.(2), the record ages τ_k are asymptotically ($n \gg 1$) effectively independent, which leads to

$$\mathbb{P}(T_{m+n} - T_m \leq T) \simeq \prod_{k=m}^{n+m-1} (1 - S(k, T)). \quad (3)$$

First, for time scales T much smaller than the typical time $T_m \propto m^{d_w}$ required to break m records and for $n \ll m$ (regime 1), Eq. (3) becomes

$$\mathbb{P}(T_{m+n} - T_m \leq T) \underset{T, n^{d_w} \ll m^{d_w}}{\propto} \exp \left[-\frac{\text{const. } n}{m^{1-\epsilon_1} T^{y_1}} \right]. \quad (4)$$

Using $T_{m+n} - T_m \propto m^{d_w - d_w^0} n^{d_w^0}$ gives the exponents of regime 1 as $y_1 = 1/d_w^0$ and $\epsilon_1 = d_w/d_w^0$. Second, for $\tau \gg n^{d_w}$ (regime 2), the memory of the n broken records no longer affects the algebraic time decay of $S(n, \tau)$, which is thus given by the persistence exponent $\theta = y_2$. Taking $m = 0$ in Eq. (3), we get

$$\mathbb{P}(T_n \leq T) \propto \exp \left[-\text{const. } n^{\epsilon_2} / T^\theta \right]. \quad (5)$$

Using $T_n \propto n^{d_w}$ leads to the exponent $\epsilon_2 = d_w \theta$.

C. Comparison with numerical simulations of non-Markovian models

We confirm the validity of our analytical results in Fig. 2 by comparing them to numerical simulations of a broad range of representative RW examples, which illustrate the classes (I), (II), and (III) of non-Markovianity discussed above. Specifically, we consider (see SI for precise definitions and Supplementary Table 1 for a summary of their characteristics): (I) (a) the fractional Brownian motion (fBm), a non-Markovian Gaussian process, with stationary increments given by $\langle (X_t - X_0)^2 \rangle = t^{2H}$, where H is the Hurst exponent; this paradigmatic

model has been used repeatedly to account for anomalous diffusion induced by long-range correlations in viscoelastic fluids [26] as well as temporal series displaying memory effects [41, 42]; (b) its extension to quenched initial conditions (qfBm), for which the statistics of increments is not stationary anymore, and which describes for instance the height fluctuations under Gaussian noise of an initially flat interface [44, 47]; (c) the elephant RW (eRW) [48], for which the current step is drawn uniformly from all of the previous steps performed by the RW, and then reversed with probability β ; (II) (d) The Self-Attractive Walk (SATW), (e) Sub-Exponential Self-Repelling Walk (SESRW) and (f) True Self-Avoiding Walk (TSAW) are prototypical examples of self-interacting RWs [49–52], for which the RW deposits a signal at each lattice site it visits and then has a transition probability depending on the number of visits to its neighbouring sites (see SI for precise rules), so that memory emerges from the interaction of the walker with the territory already visited; these RWs have been shown to be relevant in the case of living cells, where it was demonstrated experimentally that various cell types can chemically modify the extracellular matrix, which in turn deeply impact their motility [53]; (III) Two models involving an explicit spatial or temporal dependence of the steps: (g) the subdiffusive (resp. (h) the superdiffusive) Average Lévy Lorentz model (subALL and supALL, respectively) [54–56] for which the transmission (resp. reflection) probability at every site decays algebraically with the distance to the origin, and (i) the scaled Brownian motion (sBm) [57] for which the jumping rate is an algebraic function of time, and which is a paradigmatic model of subdiffusion [58].

Figure 2 reveals excellent quantitative agreement between numerical simulations and our analytical results. The data collapse of the properly rescaled record ages tail distribution and the confirmation of the two successive algebraic decays τ^{-1/d_w^0} and $\tau^{-\theta}$ show that Eq. (1) unambiguously captures the dependence on both the number of records n and the time τ (further confirmed by the analytical determination of the full tail distribution in the solvable case of the sBm, see SI). We emphasize that the very different nature of these examples (subdiffusive and superdiffusive, aging and non aging, covering all classes of non-Markovian RWs) shows the broad applicability of our approach.

DISCUSSION

We demonstrate the relevance of our results by showing that they apply even when the hidden degrees of freedom responsible for the non-Markovianity of the dynamics are unknown, as is the rule in real observations.

This is illustrated by considering both trajectories involving a variety of tracers in complex fluids (see Fig.3 (c) to (e)), which provide experimental realizations [26] of several non-Markovian RW models discussed above) and real time series in diverse fields displaying memory

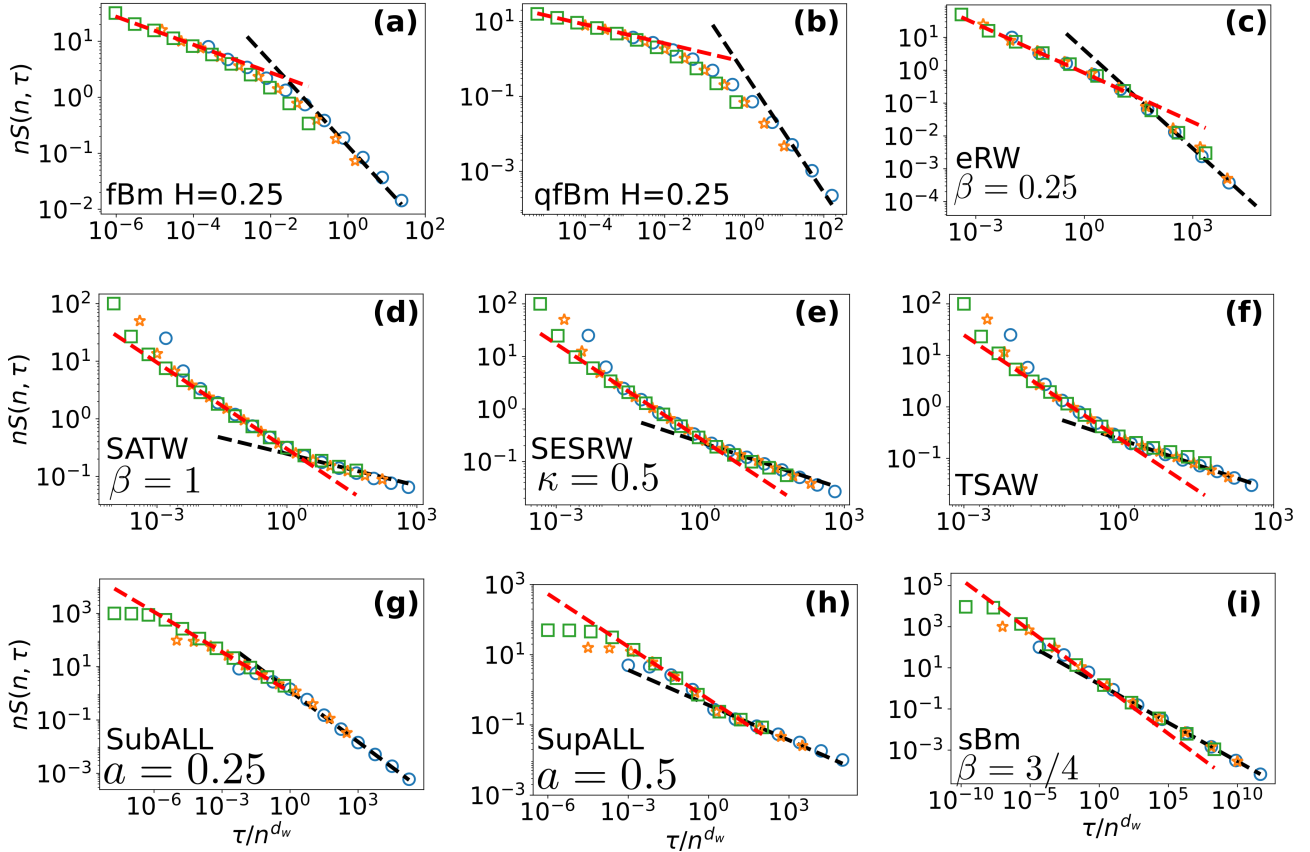


FIG. 2. **Universal record age distributions for non-Markovian RWs: theoretical predictions (lines) vs numerical simulations (symbols).** Simulated rescaled tail distribution of record ages τ_n for different values of record number n displayed for various representative RW models: **(a)** fractional Brownian motion (fBm) of Hurst exponent $H = 0.25 = 1/d_w = 1 - \theta$ for $n = 8, 16$ and 32 **(b)** quenched fBm (qfBm) of Hurst exponent $H = 0.25 = 1/d_w$ and $\theta \approx 1.55$ for $n = 5, 10$ and 20 **(c)** elephant RW (eRW) with $\beta = 0.25$ such that $d_w = 2$ and $\theta = 1$, for $n = 10, 25$ and 50 **(d)** Self-Attractive Walk (SATW) with $\beta = 1$, such that $d_w = 2$ and $\theta = e^{-1}/2$ for $n = 25, 50$ and 100 **(e)** Sub-Exponential Self-Repelling Walk (SESRW) with $\beta = 1$ and $\kappa = 0.5$ such that $d_w = 5/3$ and $\theta \approx 0.3$ for $n = 25, 50$ and 100 **(f)** True Self-Avoiding Walk (TSAW) with $\beta = 1$ such that $d_w = 3/2$ and $\theta = 1/3$ for $n = 25, 50$ and 100 **(g)** subdiffusive Average Lévy Lorentz (subALL) with $a = 0.25$ such that $d_w = 2.75$, $d_w^0 = 2$ and $\theta = 7/11$ for $n = 10, 100$ and 1000 **(h)** superdiffusive ALL (supALL) with $a = 0.5$ such that $d_w = 3/2$, $d_w^0 = 2$ and $\theta = 1/3$ for $n = 10, 100$ and 1000 **(i)** exact rescaled tail distribution (see SI) for scaled Brownian motion (sBm) with $\beta = 0.75$ such that $d_w = 8/3$, $d_w^0 = 2$ and $\theta = 3/8$ for $n = 100, 1000$ and 10000 . Increasing values of n are represented respectively by blue circles, orange stars and green squares. The black dashed line represents the algebraic decay $\tau^{-\theta}$ while the red dashed line stands for the algebraic decay τ^{-1/d_w^0} .

effects, for which record ages are crucial as they characterize the occurrence of extreme events (see Fig.3 **(a)**, **(b)** and **(f)** to **(h)**).

Specifically, we consider the following data: **(a)** river flows [32] ($1/d_w \approx 0.14$), **(b)** volcanic soil temperatures [29, 30] ($1/d_w \approx 0.42$), **(c)** trajectories of microspheres in gels [26] ($1/d_w \approx 0.43$) **(d)** trajectories of vacuoles inside an amoeba [26] ($1/d_w \approx 0.67$), **(e)** trajectories of telomeres in a nucleus [26, 59] ($1/d_w \approx 0.25$), **(f)** pyrimidines/purines DNA RW where a step value is given by the nucleotide type, +1 for adenine/thymine, -1 for cytosine/guanine [34, 35] ($1/d_w \approx 0.67$), **(g)** cumulative air temperatures [31] ($1/d_w \approx 0.8$), **(h)** cumulative Ethernet traffic [36–38] ($1/d_w \approx 0.8$). The walk dimension

d_w was estimated by applying the Detrending Moving Average (DMA) method [60, 61] to these data, which removed the deterministic behaviours (see SI for details on the datasets' analysis). Indeed, the characterization of extreme events, and thus records, requires the meticulous examination of fluctuations around the trend, as underlined in [31, 62].

We stress that we do not require any knowledge on the microscopic details of the process to obtain the record age statistics provided by Eq. (1). In particular, the processes are not necessarily Gaussian and can exhibit various distributions of the increments $x_t \equiv X_{T+t} - X_T$ (see Fig. 3), as long as they are asymptotically scale-invariant (the sampling time of the data is much longer than the

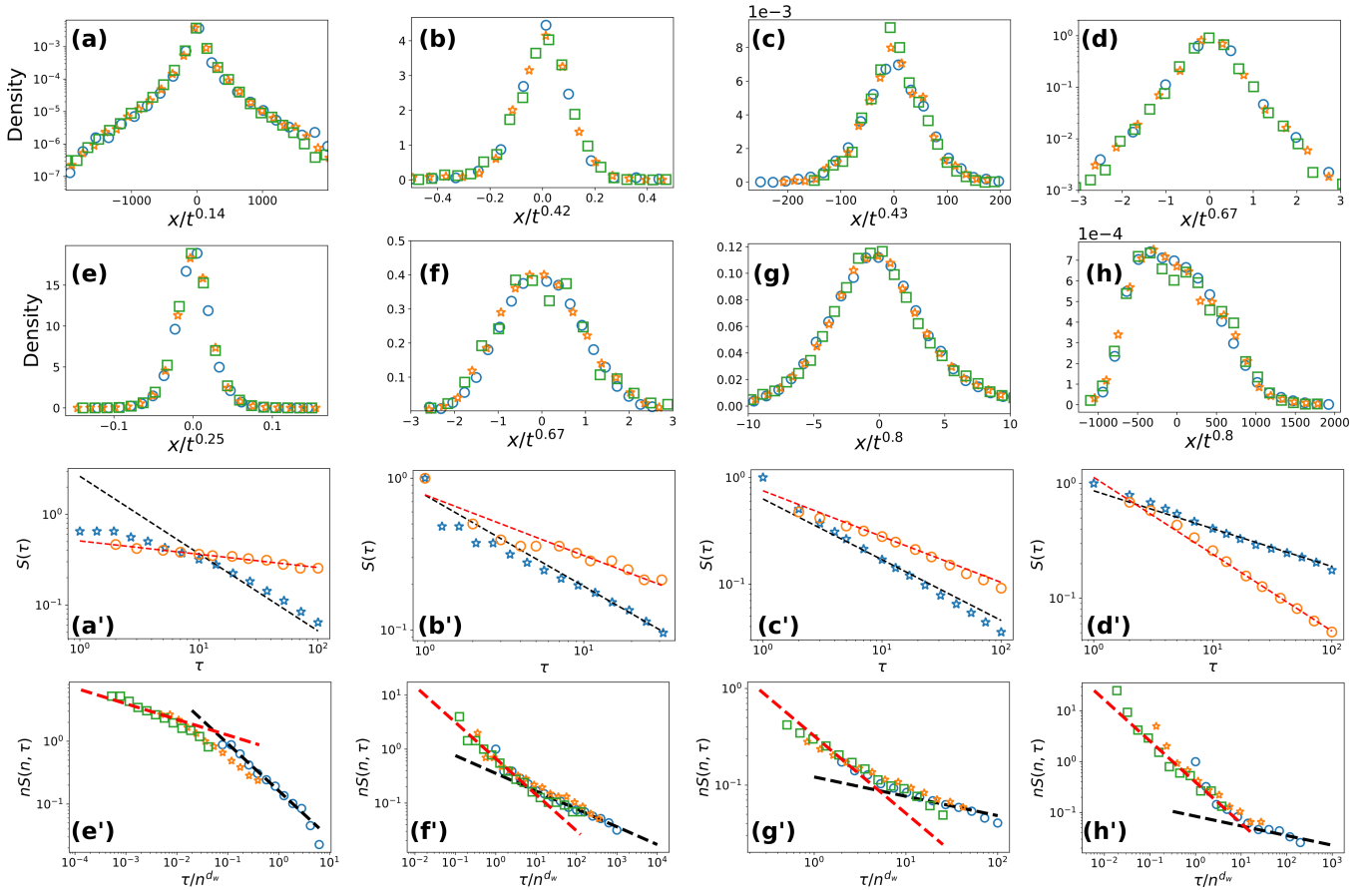


FIG. 3. **Universal record age distributions for non-Markovian RWs: theoretical predictions (lines) vs experimental RW realizations and real time observations (symbols).**

(a)-(h) Distribution of the increment $x_t = X_{t+T} - X_T$ at different times t normalised by t^{1/d_w} for: (a) river discharge ($t = 10, 20,$ and 40), (b) volcanic soil temperature ($t = 5, 10,$ and 20), (c) motion of microspheres in a gel ($t = 2, 4,$ and 8), (d) motion of vacuoles inside an amoeba ($t = 10, 20,$ and 40), (e) motion of telomeres ($t = 20, 40,$ and 80), (f) DNA RW ($t = 20, 40,$ and 80), (g) cumulative air temperature ($t = 5, 10,$ and 20), and (h) Ethernet cumulative requests ($t = 500, 1000,$ and 2000). Increasing values of times are represented successively by blue circles, orange stars and green squares.

(a')-(d') Statistics of the time to first reach the initial value in the sub interval (blue stars) and the statistics of the records (regardless of the number n of records, orange circles) for (a') river discharge, (b') volcanic soil temperature, (c') motion of microspheres in a gel, and (d') motion of vacuoles inside an amoeba. The black dashed line represents the algebraic decay τ^{-1+1/d_w} while the red dashed line stands for the algebraic decay τ^{-1/d_w} .

(e')-(h') Rescaled tail distribution of record ages τ_n for different values of the number of records n for (e') motion of telomeres ($n = 1, 3,$ and 6), (f') DNA RW ($n = 1, 2,$ and 4), (g') cumulative air temperatures ($n = 1, 2,$ and 3), and (h') Ethernet cumulative requests ($n = 1, 5,$ and 25). Increasing values of n are represented successively by blue circles, orange stars, and green squares. The lines represent the algebraic decays as for (a')-(d').

microscopic time scales involved in the process to avoid effects similar to those observed in [63], as it is checked in Sec. S3 of SI).

Figure 3 demonstrates the quantitative agreement between various real data (see SI Supplementary Figure 8 for additional datasets, including examples displaying aging of the increments x_t) and our analytical predictions given by Eq. (1). The strong dependence of record ages on the number n of records already achieved, predicted by our analytical approach and confirmed by both numerical simulations and real observations, is a direct

manifestation of the non-Markovian feature of the underlying RWs. These results quantitatively demonstrate the significance of memory effects in the record ages of non-Markovian RWs, providing the tools to better predict record-breaking events.

METHODS

Numerical simulations of non-Markovian RWs

In this section, we present briefly the models and the numerical methods used to generate the data in Fig 2.

- (a) *Fractional Brownian motion (fBm)*. The fBm is a non-Markovian Gaussian process, with stationary increments. Thus, an fBm X_t of Hurst index H is defined by its covariance

$$\text{Cov}(X_t, X_{t'}) = \frac{1}{2} (t^{2H} + t'^{2H} - |t - t'|^{2H}) . \quad (6)$$

The steps $\eta_t = X_t - X_{t-1}$ are called fractional Gaussian noise (fGn). Nowadays, the fBm is broadly spread and its implementations could be found in standard packages of python or Wolfram Mathematica.

- (b) *Quenched fBm (qfBm)*. This process is an extension of fBm to quenched initial conditions, which results in non-stationary increment statistics. In particular, it describes the height fluctuations under Gaussian noise of an initially flat interface. Then X_t corresponds to the height of the interface at position $x = 0$, $X_t = h(0, t)$, $h(x, t)$ following the Stochastic Differential Equation (SDE)

$$\partial_t h(x, t) = -(-\Delta)^{z/2} h(x, t) + \eta(x, t). \quad (7)$$

Here $\eta(x, t)$ is a Gaussian noise with possible spatial correlations. We solve numerically this SDE with a spatial discretization $\Delta x = 1$ and a time discretization $\Delta t = 0.1$. The system is initially flat, $h(x, t = 0) = 0$.

- (c) *Elephant RW (eRW)*. This process is representative of interactions with its own trajectory. At time t , the step η_t is drawn uniformly among all the previous steps η_i ($i < t$) and is reversed with probability β .
- (d) *Self-attractive walk (SATW)*. This model is a prototypical example of self-interacting RWs. In the SATW model [49–52], the RW at position i jumps to a neighbouring site $j = i \pm 1$ with probability depending on the number of times n_j it has visited site j ,

$$p(i \rightarrow j) = \frac{\exp[-\beta H(n_j)]}{\exp[-\beta H(n_{i-1})] + \exp[-\beta H(n_{i+1})]}, \quad (8)$$

where $H(0) = 0$, $H(n > 0) = 1$ and $\beta > 0$.

- (e-f) *Exponential self-repelling RW*. This is another example of self-interacting RW. In this model, the RW at position i jumps to a neighbouring site $j = i \pm 1$

with probability depending on the number of times n_j it has visited site j ,

$$p(i \rightarrow j) = \frac{\exp[-\beta n_j^\kappa]}{\exp[-\beta n_{i-1}^\kappa] + \exp[-\beta n_{i+1}^\kappa]} \quad (9)$$

where κ and β are two positive real numbers.

- (g-h) *Average Lévy Lorentz gas (ALL)*. We consider a RW on a 1d lattice with position dependent reflection or transmission probabilities $r(x)$ or $t(x)$. In the subdiffusive model (resp. superdiffusive model), the transmission coefficient $t(x)$ (resp. reflection coefficient $r(x)$) is taken to be proportional to $|x|^{a-1}$ at large distance $|x|$ from the origin.

Data analysis

In this section we provide the method developed to determine the walk dimension of the time series presented in Fig. 3 as well as numerical checks of their stationarity.

(i) *Walk dimension determination*: In order to obtain the walk dimension d_w in a time series, we apply the Detrending Moving Average (DMA) method [60, 61], which consists in evaluating the typical fluctuations in a window of size ℓ regardless of any bias or deterministic trend. More precisely, for a dataset $(X_t)_{t=0, \dots, N}$, we consider the windows of size up to ℓ_{\max} , compute the window averages $x_t^\ell = \frac{1}{\ell} \sum_{i=0}^{\ell-1} X_{t-i}$, and the typical fluctuation for a window of size ℓ , $F(\ell) = \sqrt{\frac{1}{N-\ell_{\max}} \sum_{t=\ell_{\max}}^N (X_t - x_t^\ell)^2}$. When several trajectories are available, we consider the average fluctuation over all the trajectories (for telomeres, vacuoles and microspheres in agarose data). If the data behave as a RW of walk dimension d_w , then $F(\ell) \propto \ell^{1/d_w}$. We obtain the value of $1/d_w$ via the DMA method to each dataset.

(ii) *Check of stationarity*: In order to check that the data are stationary, we compare the MSD obtained from the increments $\{x_t = X_{t+T} - X_T\}_{T \leq N/4, t}$ in the first quarter of the data and the increments $\{x_t = X_{t+T} - X_T\}_{3N/4 \leq T, t}$ in the last quarter of the data.

(iii) *Record ages in datasets*: Record ages are obtained by starting the subtrajectories at values of t equally spaced at intervals at least 200 time steps long, and observing successive records occurring in the subtrajectory. First return times are obtained by starting the subtrajectories at any value of time.

DATA AVAILABILITY

The simulation data of this study are generated based on the code deposited in a GitHub repository [65] located at <https://github.com/LeoReg/RecordAges>.

The data of the Hadley Centre Central England Temperature (HadCET) project are available at <https://www.metoffice.gov.uk/hadobs/hadcet/>. The data of the European Climate Assessment & Dataset (ECA&D) project are available at <https://www.ecad.eu/>. The volcanic soil temperature data are available at Ref. [30]. River discharge data are available at <https://portal.grdc.bafg.de/applications/>. The GenBank database is available at <https://www.ncbi.nlm.nih.gov/genbank/>. The data of traffic traces are available at <http://ita.ee.lbl.gov/html/contrib/BC.html>. Experimental trajectories of fBm realizations are available

upon request by the authors of Ref. [26]. Experimental cell migration trajectories are available upon request by the authors of Ref. [53].

CODE AVAILABILITY

The codes used to generate the simulation data presented in this study as well as the code to analyze the experimental data have been deposited in a GitHub repository located at <https://github.com/LeoReg/RecordAges>.

REFERENCES

-
- [1] Majumdar, S. N., Pal, A. & Schehr, G. Extreme value statistics of correlated random variables: a pedagogical review. *Phys. Rep.* **840**, 1–32 (2020).
- [2] Kearney, M. J. Record statistics for a discrete-time random walk with correlated steps. *J. Stat. Mech.* **2020**, 023206 (2020).
- [3] Godrèche, C. & Luck, J.-M. Record statistics of integrated random walks and the random acceleration process. *J. Stat. Phys.* **186**, 4 (2022).
- [4] Godrèche, C., Majumdar, S. N. & Schehr, G. Record statistics of a strongly correlated time series: random walks and Lévy flights. *J. Phys. A: Math. Theor.* **50**, 333001 (2017).
- [5] Kumar, A. & Pal, A. Universal framework for record ages under restart. *Phys. Rev. Lett.* **130**, 157101 (2023).
- [6] Sabhapandit, S. Record statistics of continuous time random walk. *Europhys. Lett.* **94**, 20003 (2011).
- [7] Benigni, L., Cosco, C., Shapira, A. & Wiese, K. J. Hausdorff dimension of the record set of a fractional brownian motion. *Electron. Commun. Probab.* **23**, 22 (2018).
- [8] Lacroix-A-Chez-Toine, B. & Mori, F. Universal survival probability for a correlated random walk and applications to records. *J. Phys. A: Math. Theor.* **53**, 495002 (2020).
- [9] Aliakbari, A., Manshour, P. & Salehi, M. J. Records in fractal stochastic processes. *Chaos* **27**, 033116 (2017).
- [10] Witze, A. Extreme heatwaves: Surprising lessons from the record warmth. *Nature* **608**, 464–465 (2022).
- [11] Ambraseys, N. N. Value of historical records of earthquakes. *Nature* **232**, 375–379 (1971).
- [12] Ben-Naim, E. & Krapivsky, P. L. Statistics of superior records. *Phys. Rev. E* **88**, 022145 (2013).
- [13] Coumou, D., Robinson, A. & Rahmstorf, S. Global increase in record-breaking monthly-mean temperatures. *Clim. Change* **118**, 771–782 (2013).
- [14] Chandler, K. N. The distribution and frequency of record values. *J. R. Stat. Soc. Ser. B Methodol.* **14**, 220–228 (1952).
- [15] Nevzorov, V. B. Records. *Theory Probab. Appl.* **32**, 201–228 (1988).
- [16] Eliazar, I. & Klafter, J. Record events in growing populations: Universality, correlation, and aging. *Phys. Rev. E* **80**, 061117 (2009).
- [17] Krug, J. Records in a changing world. *J. Stat. Mech.* **2007**, P07001 (2007).
- [18] Gouet, R., Lafuente, M., López, F. J. & Sanz, G. Exact and asymptotic properties of δ -records in the linear drift model. *J. Stat. Mech.* **2020**, 103201 (2020).
- [19] Majumdar, S. N. & Ziff, R. M. Universal record statistics of random walks and lévy flights. *Phys. Rev. Lett.* **101**, 050601 (2008).
- [20] Majumdar, S. N., Schehr, G. & Wergen, G. Record statistics and persistence for a random walk with a drift. *J. Phys. A: Math. Theor.* **45**, 355002 (2012).
- [21] Godrèche, C., Majumdar, S. N. & Schehr, G. Universal statistics of longest lasting records of random walks and Lévy flights. *J. Phys. A: Math. Theor.* **47**, 255001 (2014).
- [22] Ben-Naim, E. & Krapivsky, P. L. Persistence of random walk records. *J. Phys. A: Math. Theor.* **47**, 255002 (2014).
- [23] Bray, A. J., Majumdar, S. N. & Schehr, G. Persistence and first-passage properties in nonequilibrium systems. *Adv. Phys.* **62**, 225–361 (2013).
- [24] Klafter, J. & Sokolov, I. M. *First steps in random walks: from tools to applications* (OUP Oxford, 2011).
- [25] Franosch, T. *et al.* Resonances arising from hydrodynamic memory in brownian motion. *Nature* **478**, 85–88 (2011).
- [26] Krapf, D. *et al.* Spectral content of a single non-brownian trajectory. *Phys. Rev. X* **9**, 011019 (2019).
- [27] Weiss, M. Single-particle tracking data reveal anticorrelated fractional brownian motion in crowded fluids. *Phys. Rev. E* **88**, 010101 (2013).
- [28] Verevrey, J. F. *et al.* Superdiffusion dominates intracellular particle motion in the supercrowded cytoplasm of pathogenic *acanthamoeba castellanii*. *Sci. Rep.* **5**, 11690 (2015).
- [29] Di Crescenzo, A., Martinucci, B. & Mustaro, V. A model based on fractional brownian motion for temperature fluctuation in the Campi Flegrei caldera. *Fractal Fract.*

- 6, 421 (2022).
- [30] Sabbarese, C. *et al.* Continuous radon monitoring during seven years of volcanic unrest at Campi Flegrei caldera (Italy). *Sci. Rep.* **10**, 9551 (2020).
- [31] Brody, D. C., Syroka, J. & Zervos, M. Dynamical pricing of weather derivatives. *Quant. Finance* **2**, 189 (2002).
- [32] Zhang, Q., Xu, C.-Y., Chen, Y. D. & Yu, Z. Multifractal detrended fluctuation analysis of streamflow series of the Yangtze river basin, China. *Hydrol. Process.* **22**, 4997–5003 (2008).
- [33] Movahed, M. S. & Hermanis, E. Fractal analysis of river flow fluctuations. *Physica A* **387**, 915–932 (2008).
- [34] Peng, C.-K. *et al.* Long-range correlations in nucleotide sequences. *Nature* **356**, 168–170 (1992).
- [35] Peng, C.-K. *et al.* Mosaic organization of dna nucleotides. *Phys. Rev. E* **49**, 1685–1689 (1994).
- [36] Leland, W. & Wilson, D. High time-resolution measurement and analysis of lan traffic: Implications for lan interconnection. In *IEEE INFCOM'91. The conference on Computer Communications. Tenth Annual Joint Conference of the IEEE Computer and Communications Societies Proceedings*, 1360–1366 (IEEE, 1991).
- [37] Fowler, H. & Leland, W. Local area network characteristics, with implications for broadband network congestion management. *IEEE J. Sel. Areas Commun.* **9**, 1139–1149 (1991).
- [38] Leland, W. E., Taqqu, M. S., Willinger, W. & Wilson, D. V. On the self-similar nature of ethernet traffic. In *Conference proceedings on Communications architectures, protocols and applications*, 183–193 (1993).
- [39] Gabel, A. & Redner, S. Random walk picture of basketball scoring. *J. Quantitative Anal. Sports* **8** (2012).
- [40] Bouchaud, J.-P. & Georges, A. Anomalous diffusion in disordered media: Statistical mechanisms, models and physical applications. *Phys. Rep.* **195**, 127–293 (1990).
- [41] Magdziarz, M., Weron, A., Burnecki, K. & Klafter, J. Fractional brownian motion versus the continuous-time random walk: A simple test for subdiffusive dynamics. *Phys. Rev. Lett.* **103**, 180602 (2009).
- [42] Mandelbrot, B. B. & Van Ness, J. W. Fractional brownian motions, fractional noises and applications. *SIAM Rev.* **10**, 422–437 (1968).
- [43] Schulz, J. H. P., Barkai, E. & Metzler, R. Aging renewal theory and application to random walks. *Phys. Rev. X* **4**, 011028 (2014).
- [44] Levernier, N., Bénichou, O., Guérin, T. & Voituriez, R. Universal first-passage statistics in aging media. *Phys. Rev. E* **98**, 022125 (2018).
- [45] Vezzani, A., Barkai, E. & Burioni, R. Single-big-jump principle in physical modeling. *Phys. Rev. E* **100**, 012108 (2019).
- [46] Carpentier, D. & Le Doussal, P. Glass transition of a particle in a random potential, front selection in nonlinear renormalization group, and entropic phenomena in Liouville and sinh-Gordon models. *Phys. Rev. E* **63**, 026110 (2001).
- [47] Majumdar, S. N., Bray, A. J., Cornell, S. & Sire, C. Global persistence exponent for nonequilibrium critical dynamics. *Phys. Rev. Lett.* **77**, 3704 (1996).
- [48] Schütz, G. M. & Trimper, S. Elephants can always remember: Exact long-range memory effects in a non-markovian random walk. *Phys. Rev. E* **70**, 045101 (2004).
- [49] Sapozhnikov, V. B. Self-attracting walk with $\nu < 1/2$. *J. Phys. A: Math. Gen.* **27**, L151 (1994).
- [50] Davis, B. Reinforced random walk. *Probab. Theor. Rel. Fields* **84**, 203–229 (1990).
- [51] Barbier-Chebbah, A., Bénichou, O. & Voituriez, R. Anomalous persistence exponents for normal yet aging diffusion. *Phys. Rev. E* **102**, 062115 (2020).
- [52] Barbier-Chebbah, A., Bénichou, O. & Voituriez, R. Self-interacting random walks: Aging, exploration, and first-passage times. *Phys. Rev. X* **12**, 011052 (2022).
- [53] d'Alessandro, J. *et al.* Cell migration guided by long-lived spatial memory. *Nat. Commun.* **12**, 4118 (2021).
- [54] Radice, M., Onofri, M., Artuso, R. & Cristadoro, G. Transport properties and ageing for the averaged lévy-lorentz gas. *J. Phys. A: Math. Theor.* **53**, 025701 (2019).
- [55] Radice, M., Onofri, M., Artuso, R. & Pozzoli, G. Statistics of occupation times and connection to local properties of nonhomogeneous random walks. *Phys. Rev. E* **101**, 042103 (2020).
- [56] Barthelemy, P., Bertolotti, J. & Wiersma, D. S. A Lévy flight for light. *Nature* **453**, 495–498 (2008).
- [57] Lim, S. C. & Muniandy, S. V. Self-similar gaussian processes for modeling anomalous diffusion. *Phys. Rev. E* **66**, 021114 (2002).
- [58] Saxton, M. J. Anomalous subdiffusion in fluorescence photobleaching recovery: a monte carlo study. *Biophys. J.* **81**, 2226–2240 (2001).
- [59] Stadler, L. & Weiss, M. Non-equilibrium forces drive the anomalous diffusion of telomeres in the nucleus of mammalian cells. *New J. Phys.* **19**, 113048 (2017).
- [60] Höll, M., Kiyono, K. & Kantz, H. Theoretical foundation of detrending methods for fluctuation analysis such as detrended fluctuation analysis and detrending moving average. *Phys. Rev. E* **99**, 033305 (2019).
- [61] Alessio, E., Carbone, A., Castelli, G. & Frappietro, V. Second-order moving average and scaling of stochastic time series. *Eur. Phys. J. B* **27**, 197–200 (2002).
- [62] Amaya, D. *et al.* Marine heatwaves need clear definitions so coastal communities can adapt. *Nature* **616**, 29–32 (2023).
- [63] Zarfaty, L., Barkai, E. & Kessler, D. A. Discrete sampling of extreme events modifies their statistics. *Phys. Rev. Lett.* **129**, 094101 (2022).
- [64] Levernier, N., Mendes, T., Bénichou, O., Voituriez, R. & Guérin, T. Everlasting impact of initial perturbations on first-passage times of non-markovian random walks. *Nat. Commun.* **13**, 5319 (2022).
- [65] Régnier, L., Dolgushev, M. & Bénichou, O. Record ages of non-markovian scale-invariant random walks. "https://zenodo.org/badge/latestdoi/682057871" (2023).

ACKNOWLEDGEMENTS

We thank T. Guérin, N. Levernier, and G. Oshanin for helpful discussions, G. Page for careful reading of the manuscript, and S. Majumdar for mentioning the similarity between the record age statistics and the statistics of the times between visits of new sites. We are thankful to D. Krapf, M. Weiss, F. Taheri and C. Selhuber-Unkel for providing us the experimental trajectories of fBM re-

alizations used in Ref. [26]. We thank J. d'Alessandro for providing us the experimental cell migration trajectories analysed in Ref. [53]. We acknowledge the data providers in the Hadley Centre Central England Temperature (HadCET) and European Climate Assessment & Dataset (ECA&D) projects. We thank the authors of Ref. [30] for giving access to the volcanic soil temperature data. We acknowledge the Global Runoff Data Centre (GRDC), 56068 Koblenz, Germany for providing the Elbe and Rhône rivers' water debit data. We acknowledge the data providers of the GenBank database, hosted by the National Library of Medicine, as well as Jaenicke T., Diederich K.W., Haas W., Schleich J., Lichter P., Pfordt M., Bach A. and Vosberg H.P. who deposited the specific HUMBYH7 sequence used in this study. We

thank the authors of Ref. [36] for the data of traffic traces.

AUTHOR CONTRIBUTIONS

O.B., L.R. and M.D. contributed to analytical calculations. L.R. and M.D. performed numerical simulations. All the authors wrote the manuscript. O.B. conceived the research

COMPETING INTERESTS

The authors declare no competing interests.

SUPPLEMENTARY INFORMATION

Record Ages of Non-Markovian Scale-Invariant Random Walks

L. Régnier, M. Dolgushev, and O. Bénichou

CONTENTS

S1. Scaling theory	1
A. Definitions	1
B. Scale-invariance of the time T_n to break n records and of its increments	1
C. Characteristic exponents of the record age distribution	2
D. General scaling criteria showing that the correlations between record ages are asymptotically irrelevant for their maximum	3
1. Effective independence criteria	3
2. General form of $\mathbb{P}(\tau_k \geq T)$	4
3. Cross-correlations	4
4. Variance of max	5
5. Conclusion	5
S2. Non-Markovian random walks (RWs)	5
A. Definition of the non-Markovian RW models	5
B. Systematic numerical check of the scale-invariance of the time increments	7
C. Systematic numerical check of the asymptotic independence of record ages	10
S3. Data analysis	12
A. Details on the datasets used in the main text	12
B. Characterization and parametrization of the data used in the main text	12
C. Analysis of complementary datasets	14
D. Datasets displaying aging of the increments	16
Supplementary References	17

S1. SCALING THEORY

We provide here the detailed calculations corresponding to the general scaling theory developed in the main text.

A. Definitions

We assume that the random walk (RW) $(X_t)_{t=0,\dots}$ converges at large time to a continuous and non-smooth scale-invariant process. Under these conditions, the process is characterized by a walk dimension $d_w > 1$, such that $X_t \propto t^{1/d_w}$, and the random variable $X_t/t^{1/d_w}$ is independent of t . We more generally assume that X_t has scale-invariant increments with a potential ageing, meaning that, for $1 \ll t \ll T$, $X_{t+T} - X_t \propto t^{1/d_w^0} T^{\alpha/2}$. This defines the aging exponent α [S1, S2] and an effective walk dimension at short times $d_w^0 \equiv (d_w^{-1} - \alpha/2)^{-1}$.

To describe the properties of the RWs, we will use their continuous limit, which requires to introduce a microscopic cut-off either in time or space (as done in [S3]). Relying here on a spatial cut-off Δx , we consider the time T_{x_0} to first reach the level $x_0 = n\Delta x$ starting from the origin, as the continuous counterpart of the time T_n to break n records.

B. Scale-invariance of the time T_n to break n records and of its increments

First, we check that the temporal scale-invariance of X_t leads to the spatial scale-invariance of T_{x_0} . Indeed, since $X_t/t^{1/d_w}$ is asymptotically independent of time t , $X_{T_{x_0}}/T_{x_0}^{1/d_w} = x_0/T_{x_0}^{1/d_w}$ is asymptotically independent of x_0

($X_{T_{x_0}} = x_0$ because of continuity). Consequently, T_{x_0} is scale-invariant in the sense that $T_{x_0}/x_0^{d_w}$ is independent of x_0 . Taking $\Delta x = 1$ and $x_0 = n\Delta x = n$ results in the following form for the cumulative distribution:

$$\mathbb{P}(T_n \leq T) = \Phi(T/n^{d_w}) , \quad (\text{S1})$$

where the scaling function Φ is independent of T and n (see Supplementary Figure 2 for numerical check of the number of records n scale-invariance with time T for representative non-Markovian RWs).

Second, we show that the scale-invariance of the increments $X_{t+T} - X_T$, $X_{t+T} - X_T \propto t^{1/d_w - \alpha/2} T^{\alpha/2} = t^{1/d_w^0} T^{\alpha/2}$, implies the scale-invariance of $T_{x_0+x_1} - T_{x_0}$. Consider the random variable $\frac{X_{T+t} - X_T}{T^{\alpha/2} t^{1/d_w^0}}$, which is independent of t and T as long as $1 \ll t \ll T$. By replacing T by T_{x_0} and t by $T_{x_0+x_1} - T_{x_0}$, we find that

$$\frac{X_{T_{x_0+x_1}} - X_{T_{x_0}}}{T_{x_0}^{\alpha/2} (T_{x_0+x_1} - T_{x_0})^{1/d_w^0}} = \frac{x_1}{T_{x_0}^{\alpha/2} (T_{x_0+x_1} - T_{x_0})^{1/d_w^0}} ,$$

is asymptotically independent of x_0 and x_1 for $1 \ll x_1 \ll x_0$. Using that $T_{x_0}/x_0^{d_w}$ is independent of x_0 , we finally obtain that

$$\frac{T_{x_0+x_1} - T_{x_0}}{(x_1/x_0^{d_w \alpha/2})^{d_w^0}} = \frac{T_{x_0+x_1} - T_{x_0}}{x_1^{d_w^0} x_0^{d_w - d_w^0}}$$

is independent of x_0 and x_1 . In other words, we have the scale invariance of $T_{x_0+x_1} - T_{x_0}$, $T_{x_0+x_1} - T_{x_0} \propto x_1^{d_w^0} x_0^{d_w - d_w^0}$. Taking $\Delta x = 1$, $x_0 = m\Delta x$ and $x_1 = n\Delta x$ implies the scaling $T_{m+n} - T_m \propto n^{d_w^0} m^{d_w - d_w^0}$. It means that the cumulative distribution in the limit $1 \ll n \ll m$ and $1 \ll T \ll m^{d_w}$ can be written as

$$\mathbb{P}(T_{m+n} - T_m \leq T) = \Psi\left(\frac{T}{n^{d_w^0} m^{d_w - d_w^0}}\right) , \quad (\text{S2})$$

where the scaling function Ψ is independent of T , n , and m . This scale-invariance of the time increments is systematically checked numerically for a number of representative non-Markovian RWs in Supplementary Figure 3.

C. Characteristic exponents of the record age distribution

We derive the exponents governing the algebraic decay of the record age distribution $S(n, \tau)$ by elaborating the arguments sketched in the main text.

We note by τ_k the k^{th} record age or, in the continuum setting, the time to reach level $(k+1)\Delta x$ starting from the first arrival at level $k\Delta x$. T_n being the time to first reach level $n\Delta x$, it is given by the sum of the $\{\tau_k\}$,

$$T_n = \sum_{k=0}^{n-1} \tau_k . \quad (\text{S3})$$

We make the self-consistent assumption that the tail distribution of τ_k is algebraic of exponent smaller than 1. As a consequence, the sum (S3) is controlled by the largest τ_k [S4], i.e.

$$\sum_{k=0}^{n-1} \tau_k \sim \max(\tau_0, \dots, \tau_{n-1}) . \quad (\text{S4})$$

We now assume (see the next subsection for an analytical justification, as well as Supplementary Figure 4 and Supplementary Figure 5 for systematic numerical checks for a number of representative non-Markovian RWs) that the record ages τ_k involved in Eq. (S4) are asymptotically ($n \gg 1$) effectively independent, which leads to

$$\mathbb{P}(T_n \leq T) \simeq \prod_{k=0}^{n-1} \mathbb{P}(\tau_k \leq T) = \prod_{k=0}^{n-1} (1 - S(k, T)) . \quad (\text{S5})$$

We search now the exponents y_i and ϵ_i characterizing the tail distribution of τ_k , $S(k, T) \propto k^{-1+\epsilon_1} T^{-y_1}$ for $T \ll k^{d_w}$ (regime 1) and $S(k, T) \propto k^{-1+\epsilon_2} T^{-y_2}$ for $T \gg k^{d_w}$ (regime 2), see Eq. (1) of the main text.

We start with $T \gg n^{d_w}$, so that all $S(k, T)$ are in the same regime $T \gg k^{d_w}$. Using Eq. (S5),

$$\mathbb{P}(T_n \leq T) \simeq \exp \left[-\text{cste.} \sum_{k=1}^{n-1} \frac{1}{k^{1-\epsilon_2}} \frac{1}{T^{y_2}} \right] \simeq \exp \left[-\text{cste.} \frac{n^{\epsilon_2}}{T^{y_2}} \right] \quad (\text{S6})$$

The scale-invariance of T_n (Eq. (S1)) implies that $\epsilon_2/y_2 = d_w$.

Next, for $T \ll n^{d_w}$, $S(n, T) \propto n^{-1+\epsilon_1} T^{-y_1}$. By splitting the sum over k between the regions $k^{d_w} \ll T$ and $k^{d_w} \gg T$, we have

$$\begin{aligned} \mathbb{P}(T_n \leq T) &\simeq \exp \left[-\text{cste.} \sum_{k=1}^{T^{1/d_w}} \frac{1}{k^{1-\epsilon_2}} \frac{1}{T^{y_2}} - \text{cste.} \sum_{k=T^{1/d_w}}^{n-1} \frac{1}{k^{1-\epsilon_1}} \frac{1}{T^{y_1}} \right] \\ &\propto \exp \left[-\text{cste.} \frac{n^{\epsilon_1}}{T^{y_1}} \right] = \exp \left[-\text{cste.} \left(\frac{n^{\epsilon_1/y_1}}{T} \right)^{y_1} \right]. \end{aligned} \quad (\text{S7})$$

This result, together with Eq. (S1), yields $\epsilon_1/y_1 = d_w = \epsilon_2/y_2$. In particular, the survival probability of the record-ages admits a scaling form in T and k :

$$S(k, T) = \frac{1}{k} \psi(T/k^{d_w}). \quad (\text{S8})$$

To proceed further, we look at the cumulative distribution of the increments $T_{m+n} - T_m$ in the limit $1 \ll n \ll m$ and $1 \ll T \ll m^{d_w}$,

$$\begin{aligned} \mathbb{P}(T_{m+n} - T_m \leq T) &= \mathbb{P} \left(\sum_{k=m}^{n+m-1} \tau_k \leq T \right) \\ &\simeq \exp \left[-\text{cste.} \sum_{k=m}^{n+m-1} \frac{1}{k^{1-\epsilon_1}} \frac{1}{T^{y_1}} \right] \simeq \exp \left[-\text{cste.} \frac{n}{m^{1-\epsilon_1} T^{y_1}} \right] = \exp \left[-\text{cste.} \left(\frac{n^{1/y_1}}{m^{(1-\epsilon_1)/y_1} T} \right)^{y_1} \right]. \end{aligned} \quad (\text{S9})$$

Using finally Eq. (S2), we obtain $y_1 = 1/d_w^0$ and $\frac{1-\epsilon_1}{y_1} = d_w^0 - d_w$, leading to $\epsilon_1 = d_w/d_w^0$. This provides the exponents y_1 and ϵ_1 of regime 1 ($\tau_n \ll n^{d_w}$). We note that the algebraic decay of $S(n, \tau)$ holds after the time τ_n such that

$$X_{\tau_n+T_n} - X_{T_n} \propto T_n^{\alpha/2} \tau_n^{1/d_w^0} \propto (n\Delta x)^{d_w \alpha/2} \tau_n^{1/d_w^0} = (n\Delta x)^{1-d_w/d_w^0} \tau_n^{1/d_w^0} \gg \Delta x. \quad (\text{S10})$$

This gives the lower bound $\tau_n \gg n^{d_w-d_w^0}$ in Eq. (1) of the main text for regime 1.

For times $\tau_n \gg n^{d_w}$ (regime 2), the record age τ_n is much larger than the typical time needed to break all the previous records. At this time scale, the memory of the n broken records no longer affects the algebraic time decay of $S(n, \tau)$, which is thus given by the usual persistence exponent $\theta = y_2$ (defined as $\mathbb{P}(T \geq \tau) \propto \tau^{-\theta}$ where T is the time needed to reach a given value for the first time). Knowing that $\epsilon_2/y_2 = d_w$, we obtain $\epsilon_2 = d_w \theta$.

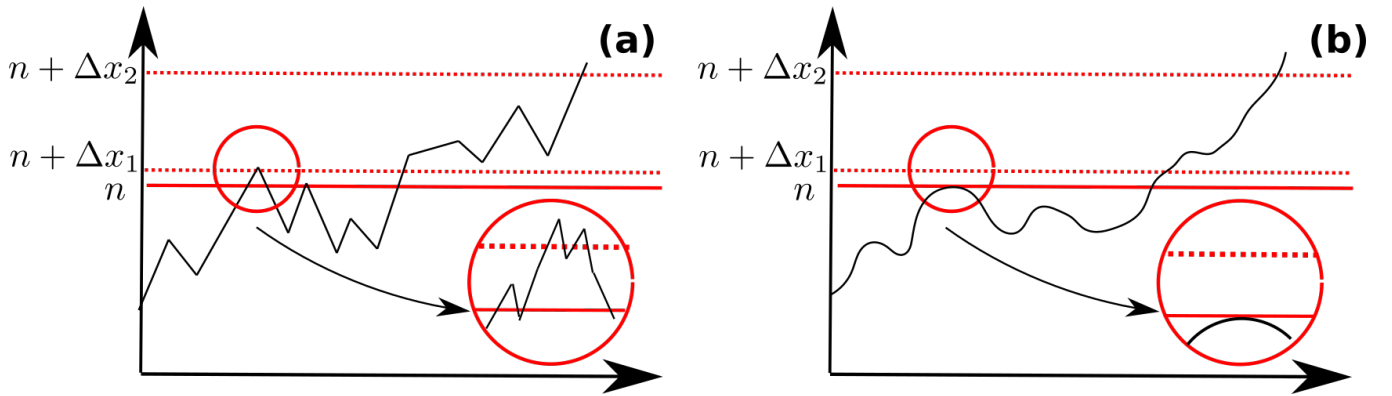
By combining the results derived in this section, we finally obtain Eq. (1) of the main text.

D. General scaling criteria showing that the correlations between record ages are asymptotically irrelevant for their maximum

1. Effective independence criteria

Here we show that in the calculation of the distribution of the maximum of the record ages, $M_n \equiv \max(\tau_0, \dots, \tau_{n-1})$, the random variables τ_k can be treated as effectively independent. To do so, we extend the criteria of Ref. [S5]. Dividing the set $(\tau_0, \dots, \tau_{n-1})$ in two subsets, $(\tau_0, \dots, \tau_{n/2-1})$ and $(\tau_{n/2}, \dots, \tau_n)$, this criteria states that the correlations between the τ_k are irrelevant if (a) the typical mean cross-correlation between the subsystems is much smaller than (b) the variance of the maximum of record ages of the whole system.

Here, however, the random variables $\{\tau_k\}$ have diverging second moments, see Eq. (1) of the main text. To overcome this difficulty, we extend the criteria of Ref. [S5] which uses variances of random variables and consider fractional moments of $\{\tau_k\}$ that converge, see below. Also, the original work of Ref. [S5] considers random variables that are Gaussian and identically distributed. Here we extend the approach to the distribution given in Eq. (1) of the main text.



Supplementary Figure 1. **Non-smoothness versus smoothness.** We compare (a) a non-smooth process to (b) a smooth process by zooming on the trajectory that reaches level n for the first time. For the non-smooth process the time needed to cross level $n + \Delta x_1$ (with a $\Delta x_1 \ll n$ small enough) starting from level n is significantly smaller than for the smooth process.

2. General form of $\mathbb{P}(\tau_k \geq T)$

We use dimensional analysis to obtain the scaling form of the tail distribution of record ages, without assuming their independence. There are no additional hypotheses on the RW processes beyond those already requested: (i) continuity, (ii) non-smoothness, and (iii) asymptotic scale-invariance.

We recall that the probability to reach level $(k + 1)\Delta x = n + \Delta x$ starting from $k\Delta x = n$ at a time larger than T is given by a function of microscopic cut-off Δx (length), the level number n (length) and T (time). Based on dimensional analysis and scale-invariance of the process, the tail distribution of the record ages takes the functional form $\mathbb{P}(\tau_k \geq T) = F(\Delta x/n, T/n^{d_w})$. We are interested in the limit $\Delta x/n \ll 1$ and $T \sim n^{d_w}$, and consider (without restriction of generality) the limit behaviour

$$\mathbb{P}(\tau_k \geq T) = F\left(\frac{\Delta x}{n}, \frac{T}{n^{d_w}}\right) \sim \left(\frac{\Delta x}{n}\right)^\beta \psi(T/n^{d_w}) \quad (\text{S11})$$

with β an exponent that we determine in the following.

For continuous non-smooth processes, when reaching the n th level, the RW crosses the level n infinitely often [S6], see Supplementary Figure 1a for an illustration. In particular, this means that when Δx is small compared to n , there is a time, much smaller than $T \sim n^{d_w}$, at which the trajectory crosses level $n + \Delta x$. Thus, the probability to reach level $n + \Delta x$ at a time larger than T goes to 0 when Δx goes to 0, which shows that the exponent β in Eq. (S11) is strictly positive, $\beta > 0$.

3. Cross-correlations

We wish to find an upper bound of the typical correlations between different τ_k of the set (τ_0, \dots, τ_n) , for example, typically quantified by the correlation between $\tau_{n/4}$ and $\tau_{3n/4}$. However, computing directly their covariance $\text{Cov}(\tau_{n/4}, \tau_{3n/4})$ would lead to a diverging result, because of a heavy-tailed τ_k distribution. Therefore, we will make use of the fractional powers of record ages, $\{\tau_k^q\}$, where the value of q allows converging second moments of these new variables.

An upper bound of the covariance $\text{Cov}(\tau_{n/4}^q, \tau_{3n/4}^q)$ is obtained by using the Cauchy-Schwarz inequality

$$\text{Cov}(\tau_{n/4}^q, \tau_{3n/4}^q) \leq \sqrt{\text{Var}(\tau_{n/4}^q) \text{Var}(\tau_{3n/4}^q)}. \quad (\text{S12})$$

The scaling behavior of each of the variances can be found based on Eq. (S11) for continuous non-smooth scale-invariant processes, leading to the moments ($k = 1, 2$)

$$\langle \tau_n^{kq} \rangle \propto n^{-\beta} \int_1^\infty d\tau \tau^{qk-1} \psi(\tau/n^{d_w}) \propto n^{-\beta+qkd_w}. \quad (\text{S13})$$

Note that for $\beta > 0$, $\langle \tau_n^{2q} \rangle$ dominates $\langle \tau_n^q \rangle^2$, so that $\text{Var}(\tau_n^q) \lesssim \langle \tau_n^{2q} \rangle$. Using this, we get the following final estimation of the upper bound for the typical cross-correlations:

$$\text{Cov} \left(\tau_{n/4}^q, \tau_{3n/4}^q \right) \leq \sqrt{\text{Var}(\tau_{n/4}^q) \text{Var}(\tau_{3n/4}^q)} \propto n^{-\beta+2qd_w}. \quad (\text{S14})$$

This last inequality finally provides an upper bound of the typical correlations between the subsets $(\tau_0, \dots, \tau_{n/2-1})$ and $(\tau_{n/2}, \dots, \tau_n)$.

4. Variance of max

The fluctuations of the maximum of the record ages $M_n \equiv \max(\tau_0, \dots, \tau_{n-1})$ are estimated by relying on the variance of $M_n^q \equiv \max(\tau_0^q, \dots, \tau_{n-1}^q)$. Based on Eqs. (S1) and (S3) and on the self-consistently checked Eq. (S4), the maximum's moments ($k = 1, 2$) can be written as:

$$\langle M_n^{kq} \rangle \sim \int_1^\infty dM M^{qk-1} (1 - \Phi(M/n^{d_w})) \propto n^{qkd_w}. \quad (\text{S15})$$

We choose q such that the integral in Eq. (S15) converges. Because M_n is scale invariant (M_n/n^{d_w} is a non-deterministic n independent random variable), we finally have

$$\text{Var}(M_n^q) \propto \langle M_n^{2q} \rangle \propto n^{2qd_w}. \quad (\text{S16})$$

5. Conclusion

We now can compare the typical cross-correlations to the fluctuations of the maximum,

$$\text{Cov} \left(\tau_{n/4}^q, \tau_{3n/4}^q \right) \leq \sqrt{\text{Var}(\tau_{n/4}^q) \text{Var}(\tau_{3n/4}^q)} \propto n^{-\beta+2qd_w} \ll n^{2qd_w} \propto \text{Var}(M_n^q). \quad (\text{S17})$$

We conclude that the fluctuations of the maximum of record ages dominate the correlations between two record ages, so that the random variables τ_k can be considered as effectively independent.

We note that, a priori, the correlations between $\{\tau_k\}$ are not negligible if one of the three hypotheses ((i) continuity, (ii) non-smoothness, and (iii) scale-invariance) breaks. While the absence of scale-invariance and of continuity would immediately invalidate calculations of this section, it is not evident for smooth processes. The necessity of the assumption of non smoothness originates from the following argument. When a realisation of a smooth process just reaches the level n , in the following the trajectory can go back to position $x < n$ without crossing level n , see Supplementary Figure 1b. Thus, for smooth processes, the probability for a RW trajectory to reach level $n + \Delta x$ at a time T for Δx arbitrary small is finite, implying $\beta = 0$ in Eq. (S11), which invalidates the estimations after it.

S2. NON-MARKOVIAN RANDOM WALKS (RWS)

A. Definition of the non-Markovian RW models

In this subsection, we present the non-Markovian random walk (RW) processes, which are used in Fig. 2 of the main text. These processes encompass the three classes of different statistical mechanisms giving rise to a non-Markovian evolution discussed in the main text and depicted in Fig. 1 of the main text. Supplementary Table 1 provides a summary of their characteristic parameters, namely d_w , α , d_w^0 and θ .

- (a) *Fractional Brownian motion (fBm)*. The fBm is a non-Markovian Gaussian process, with stationary increments. Thus, an fBm X_t of Hurst index H is defined by its covariance

$$\text{Cov}(X_t, X_{t'}) = \frac{1}{2} (t^{2H} + t'^{2H} - |t - t'|^{2H}). \quad (\text{S18})$$

The steps $\eta_t = X_t - X_{t-1}$ are called fractional Gaussian noise (fGn). Nowadays, the fBm is broadly spread and its implementations could be found in standard packages of python or Wolfram Mathematica. Besides, the survival probability of fBm is characterized by the persistence exponent $\theta = 1 - H$, which was derived in [S8–S10].

Model	d_w	α	$1/d_w^0$	θ
fBm	$1/H$	0	H	$1 - H$
qfBm	$1/H$	0	H	$\theta(H)$ (see [S7])
eRW	2	0	1/2	$3/2 - 2\beta$
SATW	2	0	1/2	$e^{-\beta}/2$
SESRW	$\frac{2+\kappa}{1+\kappa}$	0	$\frac{2+\kappa}{1+\kappa}$	≈ 0.3
TSAW	3/2	0	3/2	1/3
subALL	$3 - a$	$\frac{a-1}{3-a}$	1/2	$(2 - a)/(3 - a)$
supALL	$1 + a$	$\frac{1-a}{1+a}$	1/2	$a/(1 + a)$
sBm	$2/\beta$	$\beta - 1$	1/2	$\beta/2$

Supplementary Table 1. Summary of the non-Markovian models considered in this study and of their characteristic parameters.

- (b) *Quenched fBm (qfBm)*. This process is an extension of fBm to quenched initial conditions, which results in non-stationary increment statistics. In particular, it describes the height fluctuations under Gaussian noise of an initially flat interface. Then X_t corresponds to the height of the interface at position $x = 0$, $X_t = h(0, t)$, $h(x, t)$ following the Stochastic Differential Equation (SDE)

$$\partial_t h(x, t) = -(-\Delta)^{z/2} h(x, t) + \eta(x, t). \quad (\text{S19})$$

Here $\eta(x, t)$ is a Gaussian noise with possible spatial correlations. We solve numerically this SDE with a spatial discretization $\Delta x = 1$ and a time discretization $\Delta t = 0.1$. The system is initially flat, $h(x, t = 0) = h_0$. The model at $z = 2$ with space-independent noise is a non-stationary fBm of Hurst exponent $H = (1 - 1/z)/2 = 1/4$ which corresponds to the continuous limit of a solid-on-solid model [S11]. The persistence exponent θ was numerically estimated to be $\theta = 1.55 \pm 0.02$ [S7].

- (c) *Elephant RW (eRW)*. This process is representative of interactions with its own trajectory. At time t , the step η_t is drawn uniformly among all the previous steps η_i ($i < t$) and is reversed with probability β . The persistence exponent was determined in [S12] to be $\theta = 3/2 - 2\beta$.
- (d) *Self-attractive walk (SATW)*. This model is a prototypical example of self-interacting RWs. In the SATW model [S12–S15], the RW at position i jumps to a neighbouring site $j = i \pm 1$ with probability depending on the number of times n_j it has visited site j ,

$$p(i \rightarrow j) = \frac{\exp[-\beta H(n_j)]}{\exp[-\beta H(n_{i-1})] + \exp[-\beta H(n_{i+1})]}, \quad (\text{S20})$$

where $H(0) = 0$, $H(n > 0) = 1$ and $\beta > 0$. It was shown in [S12] that the persistence exponent of this RW is given by $e^{-\beta}/2$.

- (e-f) *Exponential self-repelling RW*. This is another example of self-interacting RW. In this model, the RW at position i jumps to a neighbouring site $j = i \pm 1$ with probability depending on the number of times n_j it has visited site j ,

$$p(i \rightarrow j) = \frac{\exp[-\beta n_j^\kappa]}{\exp[-\beta n_{i-1}^\kappa] + \exp[-\beta n_{i+1}^\kappa]} \quad (\text{S21})$$

where κ and β are two positive real numbers. It was shown [S16] that the walk dimension of such walks is given by $d_w = \frac{1+\kappa}{2+\kappa}$. In the case $\kappa = 1$ (the True Self-Avoiding Walk, TSAW, [S17–S19]), the persistence exponent is given by [S15] $\theta = 1/3$, while for $\kappa < 1$ (the Sub-Exponential Self-repelling Walk, SESRW, [S16, S20]), its numerical estimation is $\theta \approx 0.3$.

(g-h) *Average Lévy Lorentz gas (ALL)*. This model is emblematic for RWs with spatially-dependent steps; Its different properties are described in [S21, S22]. We consider a RW on a $1d$ lattice with position dependent reflection or transmission probabilities $r(k)$ or $t(k)$. In the subdiffusive model (subALL), the transmission coefficient is taken to be

$$t(k) = \begin{cases} \frac{a \sin(\pi a) \zeta(1+a)}{2\pi |k|^{1-a}} & \text{if } |k| > 0 \\ 1/2 & \text{otherwise} \end{cases} \quad (\text{S22})$$

In the continuous setting, this is equivalent to a space dependent diffusion coefficient for $0 < a < 1$, $D_a(x) = (4\Lambda|x|^{1-a} - 2)^{-1}$ where $\Lambda = \frac{\pi}{a \sin(\pi a) \zeta(1+a)}$. The persistent exponent is given by $\theta = 1 - 1/(3+a)$ [S22]. In the superdiffusive model (supALL), the reflection coefficient is taken to be

$$r(k) = \begin{cases} \frac{a \sin(\pi a) \zeta(1+a)}{2\pi |k|^{1-a}} & \text{if } |k| > 0 \\ 1/2 & \text{otherwise.} \end{cases} \quad (\text{S23})$$

In the continuous setting, this is equivalent to a space dependent diffusion coefficient for $0 < a < 1$, $D_a(x) = \Lambda|x|^{1-a} - 1/2$ where $\Lambda = \frac{\pi}{a \sin(\pi a) \zeta(1+a)}$. The persistent exponent is given by $\theta = 1 - 1/(1+a)$ [S22].

(i) *Scaled Brownian motion (sBm)*. The sBm model represents RWs with time-dependent steps [S23–S26]. Starting from X_t^0 a process with i.i.d. symmetric jumps η_t^0 with finite variance, we define the scale process of parameter β by $X_t \equiv X_{\lfloor t^\beta \rfloor}^0$, or equivalently $\eta_t = \sum_{k=\lfloor (t-1)^\beta \rfloor}^{\lfloor t^\beta \rfloor - 1} \eta_k^0$. A second way to define the sBm on discrete times is to consider steps η_t following a binomial distribution of parameters $(N_t, 1/2)$ where N_t is Poisson distributed of average $\lambda(t) = t^{\beta-1}$ (the one used in Supplementary Figure 2). In the continuous setting, it amounts to a time-dependent overdamped Langevin equation,

$$\frac{dX_t}{dt} = \sqrt{2D\beta t^{\beta-1}} \eta_t, \quad (\text{S24})$$

where η_t is a white noise of unit variance. The persistence exponent of sBm is $\theta = \beta/2$ [S24].

The sBm model allows one to compute the distribution of $\tau_{x_0} \equiv T_{x_0+\Delta x} - T_{x_0}$ analytically in the continuous limit,

$$\begin{aligned} \mathbb{P}(\tau_{x_0} \geq \tau) &= \int_0^\infty dT_0 \mathbb{P}(T_{x_0}^0 = T_0) \mathbb{P}(T_{\Delta x}^0 \geq (\tau + T_0^{1/\beta})^\beta - T_0) \\ &= \int_0^\infty dT_0 \frac{x_0}{\sqrt{2\pi T_0^3}} \exp\left[-\frac{x_0^2}{2T_0}\right] \operatorname{erf}\left(\frac{\Delta x \sqrt{2}}{\sqrt{(\tau + T_0^{1/\beta})^\beta - T_0}}\right) \end{aligned} \quad (\text{S25})$$

We plot this exact formula in Fig. 2 of the main text ($x_0 = n$, $\Delta x = 1$) and in Supplementary Figure 3 ($x_0 = m$, $\Delta x = n$). In the case of small Δx ,

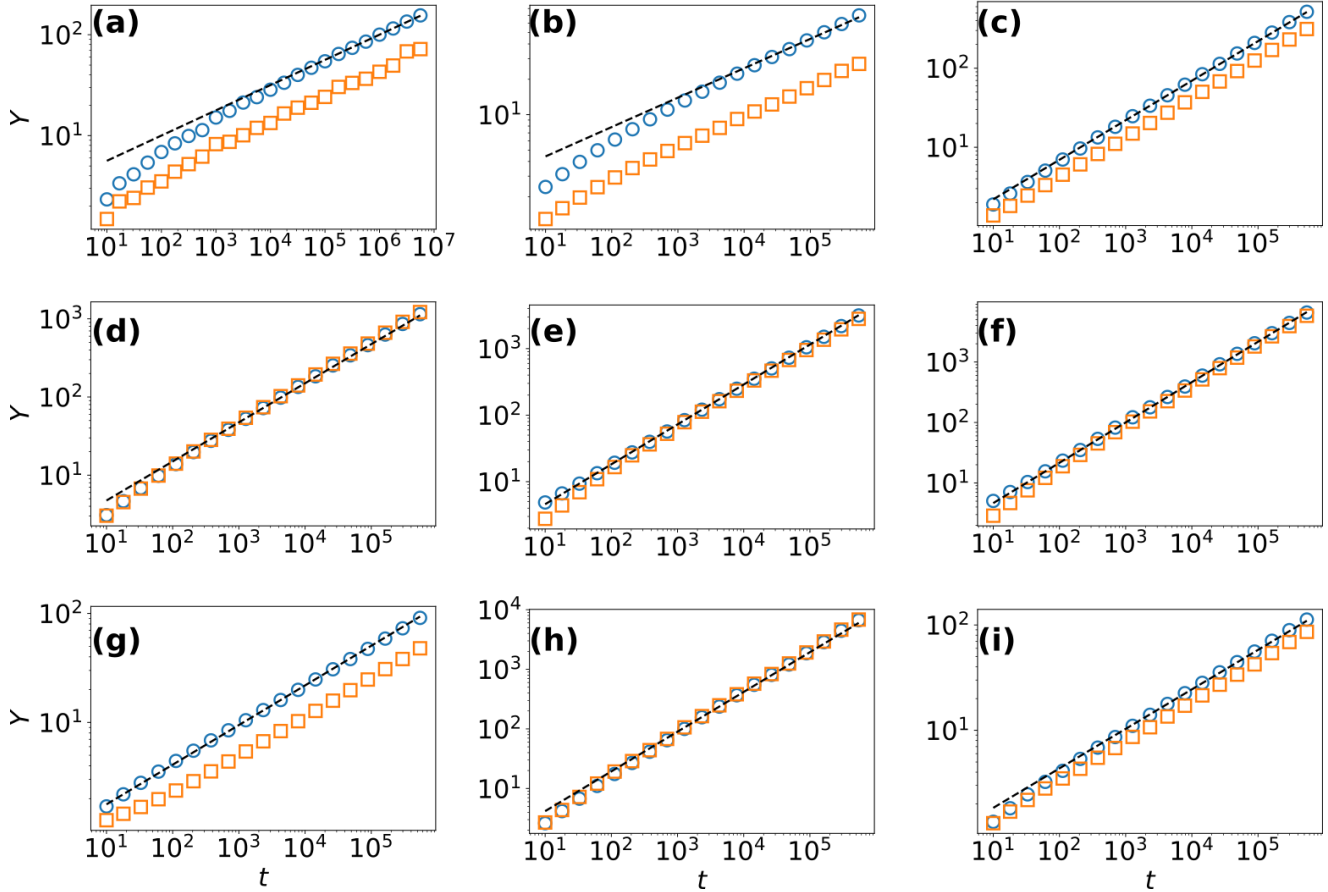
$$\mathbb{P}(\tau_{x_0} \geq \tau) \sim \frac{2\Delta x}{\pi} \int_0^\infty dT_0 \frac{x_0}{\sqrt{T_0^3}} \exp\left[-\frac{x_0^2}{2T_0}\right] \frac{1}{\sqrt{(\tau + T_0^{1/\beta})^\beta - T_0}} \propto \begin{cases} \frac{\Delta x}{\sqrt{\tau x_0^{1-1/\beta}}} & \text{for } \tau \ll x_0^{2/\beta}, \\ \frac{\Delta x}{\tau^{\beta/2}} & \text{for } \tau \gg x_0^{2/\beta}, \end{cases} \quad (\text{S26})$$

in full agreement with the central result of this work, Eq. (1) of the main text.

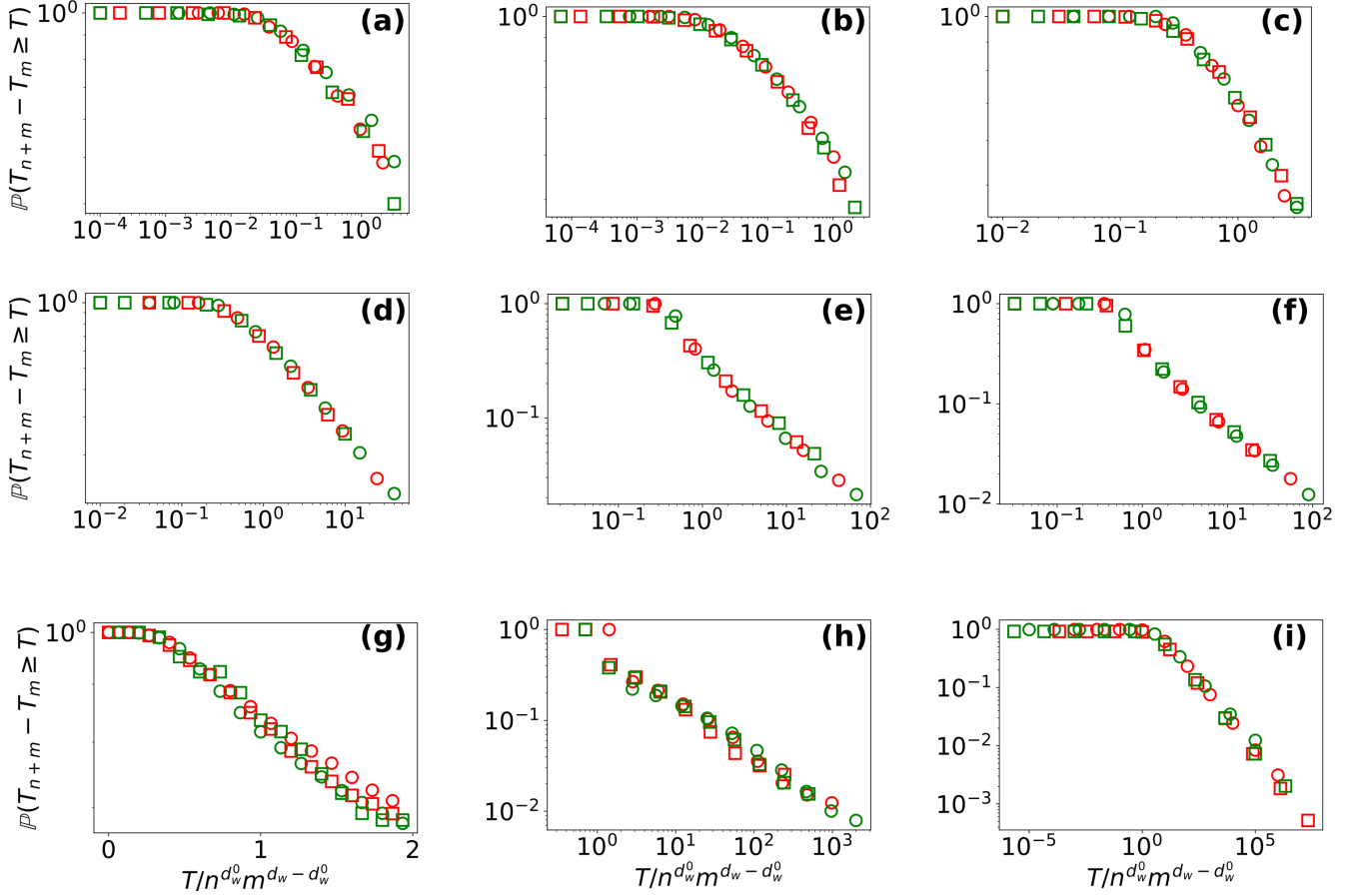
B. Systematic numerical check of the scale-invariance of the time increments

Based on the RW models described above, we confirm the scale invariance of the following random variables :

- *The number of records.* We show in Supplementary Figure 2 that the number of records at time t is indeed scale invariant at large times as its average and standard deviation grow as expected as t^{1/d_w} for all non-Markovian process considered.
- *The time-increments between records.* Supplementary Figure 3 provides the distributions of the time increments $T_{m+n} - T_m$ and checks their scale invariance with respect to m and n ; namely, that $(T_{m+n} - T_m)/n^{d_w^0} m^{d_w - d_w^0}$ is independent of m and n for $n \ll m$.



Supplementary Figure 2. **Average and standard deviation of number of records.** Each subpanel represents the average (blue circles) and standard deviation (orange squares) of the number of records reached at time t compared to the scaling expectation $\propto t^{1/d_w}$ (dashed lines) for **(a)** fractional Brownian motion (fBm) of Hurst exponent $H = 0.25 = 1/d_w$, **(b)** quenched fBm (qfBm) of Hurst exponent $H = 0.25 = 1/d_w$, **(c)** elephant RW (eRW) of parameter $\beta = 0.25$ such that $d_w = 2$, **(d)** Self-Attractive Walk (SATW) of parameter $\beta = 1$, such that $d_w = 2$, **(e)** Sub-Exponential Self-Repelling Walk (SESRW) of parameter $\beta = 1$ and $\kappa = 0.5$ such that $d_w = 5/3$, **(f)** True Self-Avoiding Walk (TSAW) of parameter $\beta = 1$ such that $d_w = 3/2$, **(g)** Subdiffusive Average Lévy Lorentz (subALL) of parameter $a = 0.25$ such that $d_w = 2.75$, $d_w^0 = 2$, **(h)** Superdiffusive Average Lévy Lorentz (supALL) of parameter $a = 0.5$ such that $d_w = 3/2$, $d_w^0 = 2$, and **(i)** Scaled Brownian motion (sBm) of parameter $\beta = 0.75$ such that $d_w = 8/3$.

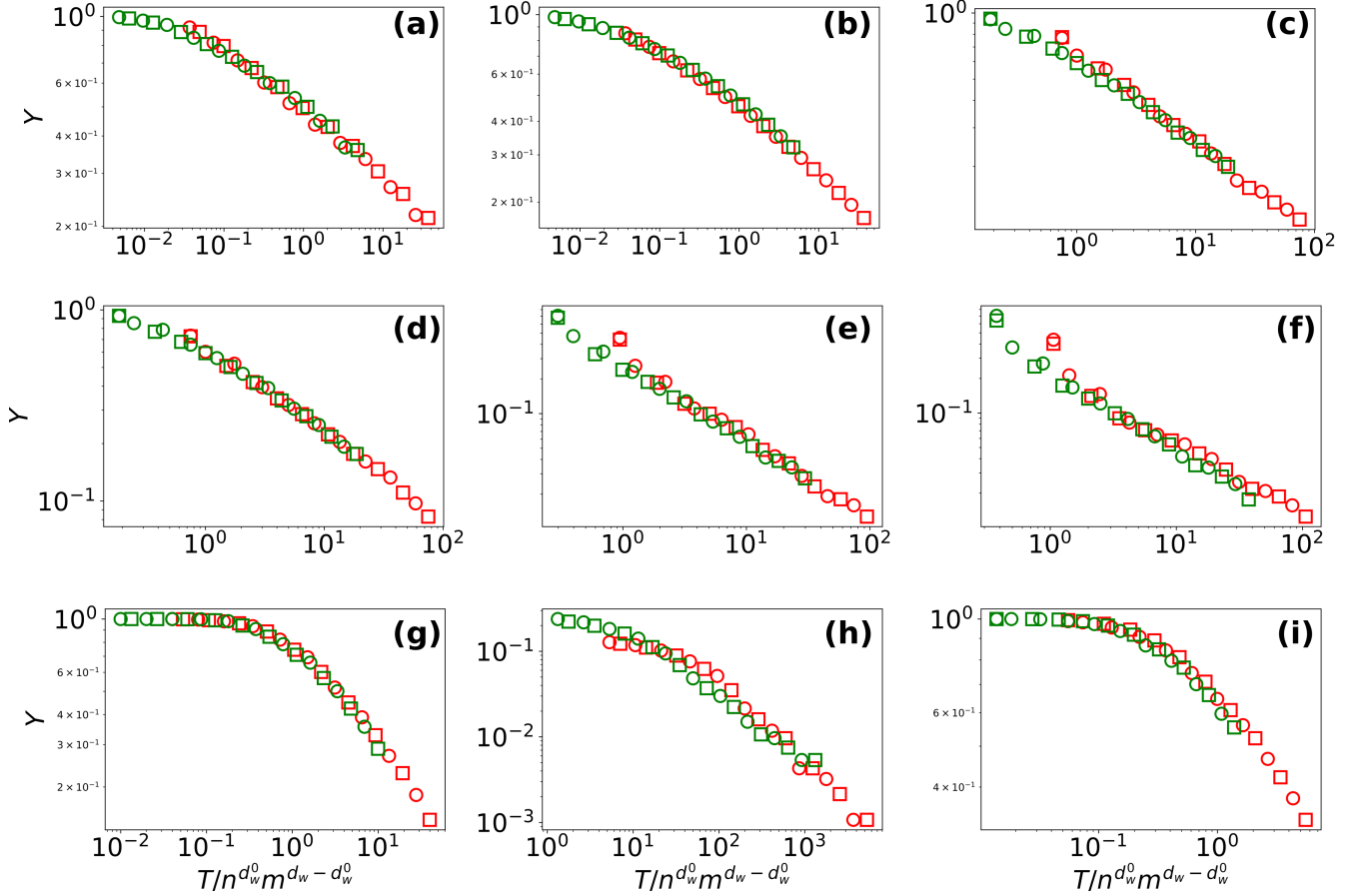


Supplementary Figure 3. **Scaled distribution of the time increments** $T_{m+n} - T_m$. Each subpanel represents the simulated tail distribution of the random variable $T_{m+n} - T_m$ as a function of $T/n^{d_w^0} m^{d_w - d_w^0}$ for different values of n and m for **(a)** fBm of Hurst exponent $H = 0.25 = 1/d_w$ ($n = 5$ and 10 , $m = 50$ and 100) **(b)** qfBm of Hurst exponent $H = 0.25 = 1/d_w$ ($n = 5$ and 10 , $m = 50$ and 100) **(c)** eRW of parameter $\beta = 0.25$ such that $d_w = 2$ ($n = 5$ and 10 , $m = 50$ and 100) **(d)** SATW of parameter $\beta = 1$, such that $d_w = 2$ ($n = 5$ and 10 , $m = 100$ and 500) **(e)** SESRW of parameter $\beta = 1$ and $\kappa = 0.5$ such that $d_w = 5/3$ ($n = 5$ and 10 , $m = 100$ and 500) **(f)** TSAW of parameter $\beta = 1$ such that $d_w = 3/2$ ($n = 5$ and 10 , $m = 100$ and 500) **(g)** subALL of parameter $a = 0.25$ such that $d_w = 2.75$, $d_w^0 = 2$ ($n = 10$ and 20 , $m = 400$ and 800) **(h)** supALL of parameter $a = 0.5$ such that $d_w = 3/2$, $d_w^0 = 2$ ($n = 5$ and 10 , $m = 50$ and 100) **(i)** Exact tail distribution for sBm of parameter $\beta = 0.75$ such that $d_w = 8/3$ ($n = 10$ and 100 , $m = 1000$ and 10000). Increasing values of m are represented respectively by red and green symbols, while increasing values of n are represented respectively by circles and squares. Times $T_m > 10^6$ are discarded to have finite computation times.

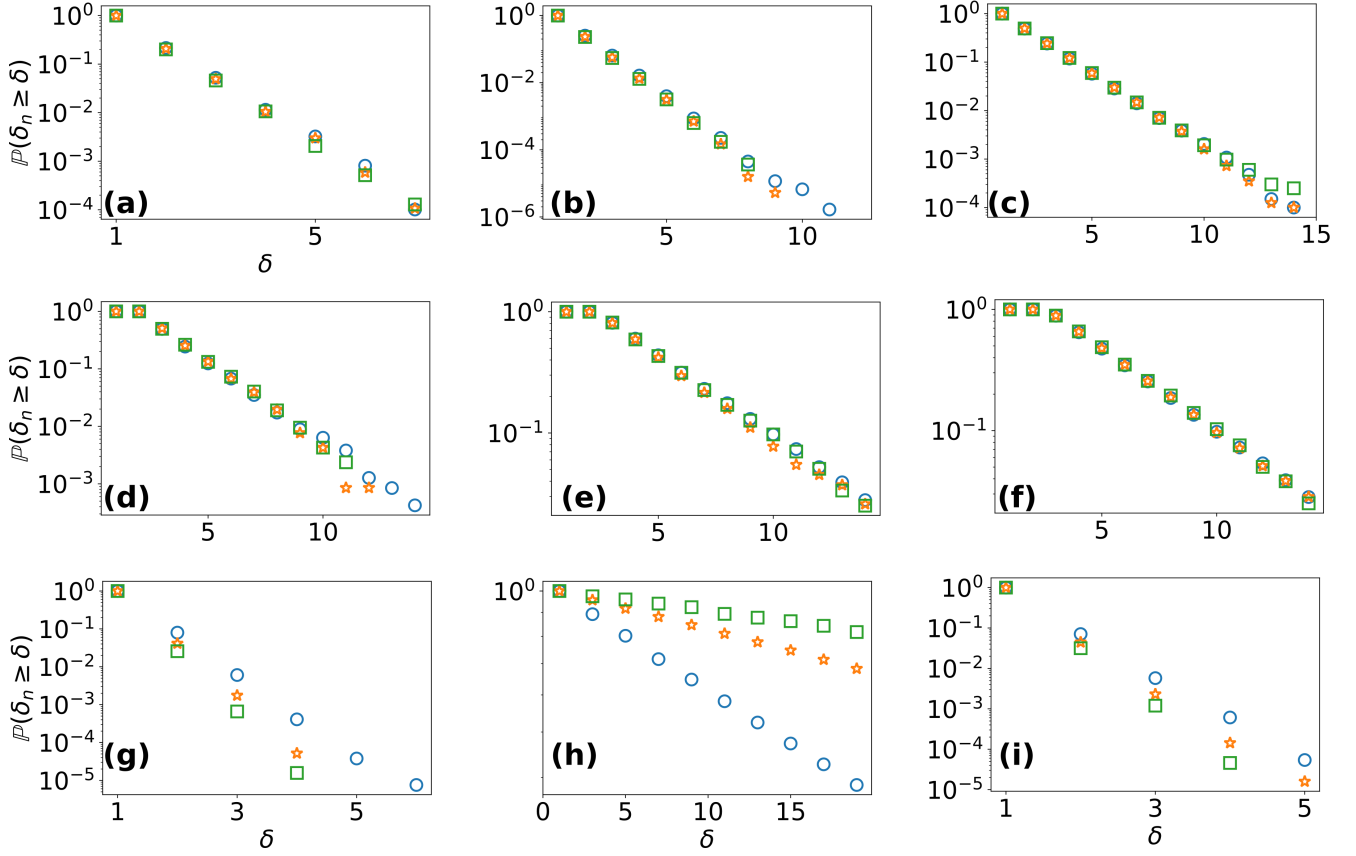
C. Systematic numerical check of the asymptotic independence of record ages

Based on the RW models described above, we make systematic tests of the independence hypothesis between record ages:

- In Supplementary Figure 4, we check the effective independence hypothesis used in Eq. (3) of the main text, by comparing $\mathbb{P}(\max(\tau_m, \dots, \tau_{m+n-1}) \leq T)$ with $\prod_{k=m}^{n+m-1} (1 - S(k, T))$ for various values of n in the regime n^{d_w} and T small in comparison to m^{d_w} . The functional forms being the same for both distributions even for different values of n (by rescaling with n and m), this confirms numerically the approximation for all the non-Markovian models considered.
- In Supplementary Figure 5, we display the probability to make at least δ successive records (event called a record run of length δ) when n record runs have been performed. In other words, we look at the joint distribution $\{\tau_n = 1, \dots, \tau_{n+k} = 1\}$, which shows an exponential decay in the correlations between successive record ages, and thus provides an additional numerical check of the independence of τ_k . We note that the time decay rate of the exponential varies with n for aging RWs, as expected from the dependency on the number n of records of the early time regime for the record age τ_n .



Supplementary Figure 4. **Scaled distribution of the record maximum with and without the independence approximation.** Each subpanel represents the tail distribution of the random variable $\max(\tau_m, \dots, \tau_{n+m-1})$, $\mathbb{P}(\tau_k > T, k = m, \dots, n + m - 1) = 1 - \mathbb{P}(\tau_k \leq T, k = m, \dots, n + m - 1)$ (circles), and the product tail distribution of $\tau_m, \dots, \tau_{n+m-1}$, $1 - \prod_{k=m}^{n+m-1} \mathbb{P}(\tau_k \leq T)$ (squares), as a function of $T/n^{d_w^0} m^{d_w - d_w^0}$ with $n = 2$ (red), $n = 4$ (green) and $m = 50$ for (a) fBm of Hurst exponent $H = 0.25 = 1/d_w$, (b) qfBm of Hurst exponent $H = 0.25 = 1/d_w$ ($n = 2$ and 4), (c) eRW of parameter $\beta = 0.25$ such that $d_w = 2$, (d) SATW of parameter $\beta = 1$, such that $d_w = 2$, (e) SESRW of parameter $\beta = 1$ and $\kappa = 0.5$ such that $d_w = 5/3$, (f) TSAW of parameter $\beta = 1$ such that $d_w = 3/2$, (g) SubALL of parameter $a = 0.25$ such that $d_w = 2.75$, $d_w^0 = 2$, (h) SupALL of parameter $a = 0.5$ such that $d_w = 3/2$, $d_w^0 = 2$, and (i) sBm of parameter $\beta = 0.75$ such that $d_w = 8/3$. Times $T_{m+n} > 10^6$ are discarded to have finite computation times.



Supplementary Figure 5. **Distributions of record runs.** Each subpanel represents the distribution of a record run δ_n for different values of the number n of previous record runs for (a) fBm of Hurst exponent $H = 0.25 = 1/d_w$, (b) qfBm of Hurst exponent $H = 0.25 = 1/d_w$, (c) eRW of parameter $\beta = 0.25$ such that $d_w = 2$, (d) SATW of parameter $\beta = 1$, such that $d_w = 2$, (e) SESRW of parameter $\beta = 1$ and $\kappa = 0.5$ such that $d_w = 5/3$, (f) TSAW of parameter $\beta = 1$ such that $d_w = 3/2$, (g) subALL of parameter $a = 0.25$ such that $d_w = 2.75$, $d_w^0 = 2$, (h) supALL of parameter $a = 0.5$ such that $d_w = 3/2$, $d_w^0 = 2$, and (i) sBm of parameter $\beta = 0.75$ such that $d_w = 8/3$. All distributions are computed for $n = 10, 25$ and 50 record runs (blue circles, orange stars and green squares). Times to reach n record runs larger than 10^6 are discarded to have finite computation times.

S3. DATA ANALYSIS

We provide a comprehensive description of the datasets used in this study, along with the general methodology that yields the results presented in the main text. Furthermore, we include complementary datasets that provide additional confirmation of our findings, including cases involving aging time series.

A. Details on the datasets used in the main text

Here, we present the datasets used in the main text:

- (a) *Elbe river discharge (m^3/s)*. We consider the daily mean debit of the Elbe river measured in Dresden [S27]. It was observed that this quantity presents correlation which can be modeled by subdiffusive non-Markovian RWs [S28]. In this time series, we obtain $H \approx 0.14$ by application of the DMA method [S29, S30], see below.
- (b) *Volcanic soil temperature ($^{\circ}C$)*. It was shown in [S31, S32] that the soil temperature monitored in the volcanic caldera of the Campi Flegrei area in Naples follows an fBm of parameter $H \approx 0.42$ once the data have been detrended by removing the linear trends between two temperature extrema (between two solstices). Here we also detrend the data by removing the same linear seasonal trends. We display the data measured at the Monte Olibano (OLB) site.
- (c) *Trajectories of microspheres in agarose gel (nm)*. The trajectories [S33] represent the $2d$ motion of 50-nm polystyrene microspheres in agarose hydrogel (we consider that x and y displacement are i.i.d., giving us 2 independent $1d$ trajectories). There are 20 trajectories of 2000 frames which were analyzed in [S33] who obtained $1/d_w \approx 0.43$.
- (d) *Motion of amoeba intracellular vacuoles (pixels = 106nm)*. We consider vacuole intracellular trajectories inside the amoeba in a $2d$ plane (we consider that x and y displacement are i.i.d., giving us 2 independent $1d$ trajectories) of at least 2048 frames. It was estimated in [S33] that the walk dimension verifies $1/d_w \approx 0.67$.
- (e) *Trajectories of telomeres (μm)*. We use $2d$ trajectories [S33] of telomeres in the nucleus of untreated U2OS cells obtained in Ref. [S34] (we consider that x and y displacement are i.i.d., giving us 2 independent $1d$ trajectories). Similarly to Ref. [S33], we only consider trajectories where the mean-square displacement grows as $t^{0.5 \pm 0.05}$, which corresponds to $1/d_w \approx 0.25$.
- (f) *DNA RW on the Homo sapiens β -myosin heavy chain (HUMBMYH7)*. It was observed in [S35, S36] that the process is a RW with long-range correlations of Hurst exponent $H \approx 0.67$. We estimate and remove the bias $\hat{v} = \frac{1}{N} \sum_{t=1}^N \eta_t$ in the data by replacing η_t by $\eta_t - \hat{v}$.
- (g) *Cumulative London air temperature ($^{\circ}C.day$)*. In this case, the temperature fluctuations (as for (b), we remove the linear trends between two solstices) are fractional Gaussian noise (fGn), in agreement to what was observed in [S37], of Hurst exponent $H \approx 0.8$ obtained via the DMA method [S29, S30], see below. We consider the cumulative temperature fluctuation, which is then fBm. This quantity is of a particular interest in the studies of derivative pricing (see [S37]).
- (h) *Cumulative Ethernet traffic (10 bytes.ms)*. The dataset represents the number of packets going through an Ethernet cable every 10 ms at the Bellcore Morristown Research and Engineering facility [S38]. In particular, in [S39], it was shown that the process is a fGn of dimension $H \approx 0.8$. As for (e), the cumulative number of requests up to a given time t gives a non-Markovian process. We detrend the cumulative data as for (g) by removing the estimated bias \hat{v} at every step. We display the measurement performed in August 1989.

B. Characterization and parametrization of the data used in the main text

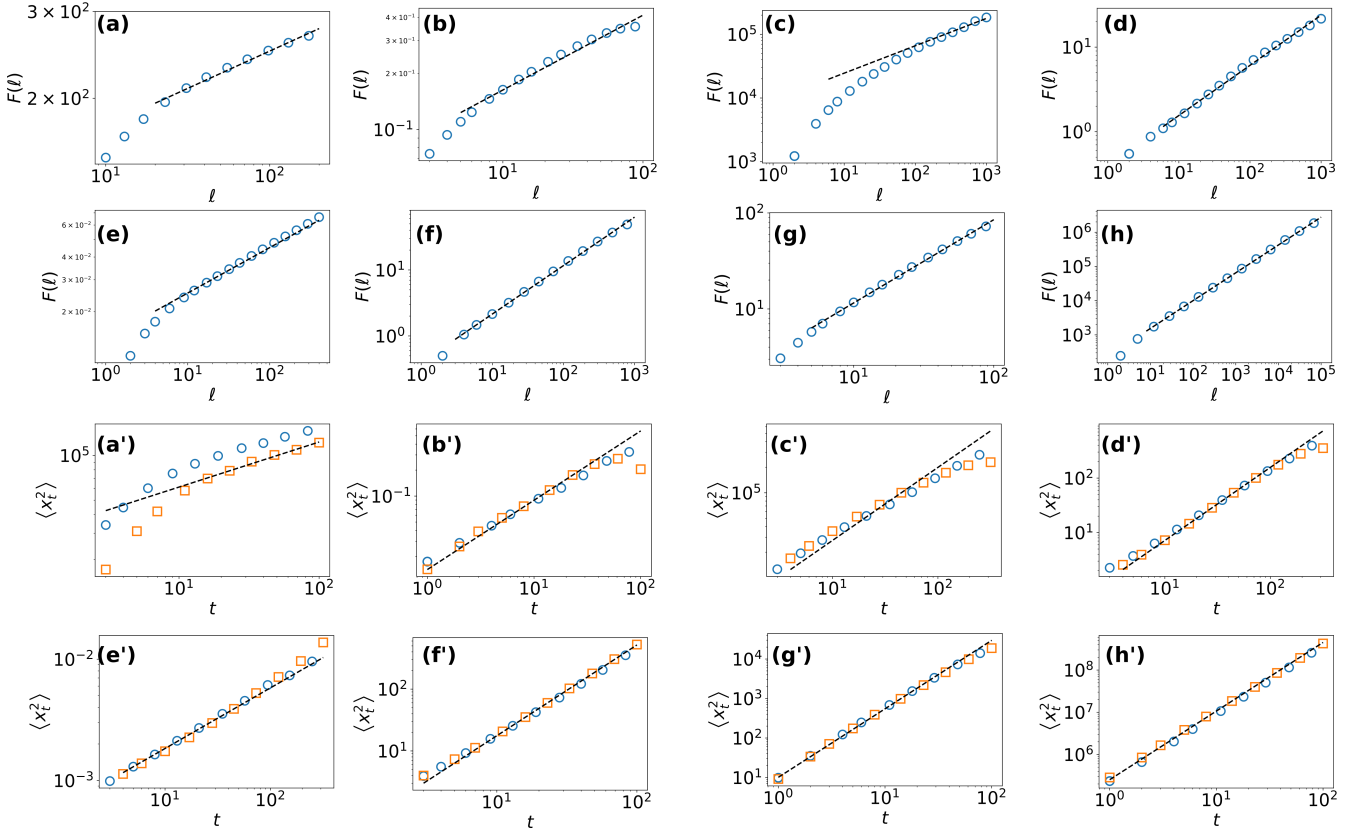
In this section we provide the method developed to determine the walk dimension of the time series presented in the main text as well as numerical checks of their stationarity.

In order to obtain the walk dimension d_w in a time series, one applies the celebrated Detrending Moving Average (DMA) [S29, S30] method, which consists in evaluating the typical fluctuations in a window of size ℓ regardless of any bias or deterministic trend. More precisely, for a dataset $(X_t)_{t=0, \dots, N}$, we consider the windows of size

up to ℓ_{\max} , compute the window averages $x_t^\ell = \frac{1}{\ell} \sum_{i=0}^{\ell-1} X_{t-i}$, and the typical fluctuation for a window of size ℓ , $F(\ell) = \sqrt{\frac{1}{N-\ell_{\max}} \sum_{t=\ell_{\max}}^N (X_t - x_t^\ell)^2}$. When several trajectories are available, we consider the average fluctuation over all the trajectories (for telomeres, vacuoles and microspheres in agarose data). If the data behave as a RW of walk dimension d_w , then $F(\ell) \propto \ell^{1/d_w}$. We obtain the value of $1/d_w$ via the DMA method (first two lines in Supplementary Figure 6). Then, we compare the exponent with that obtained from the Mean Square Displacement (MSD). As one can see in the last two lines of Supplementary Figure 6, the MSD has the algebraic growth predicted by the DMA method, which indicates that the deterministic trends have been removed correctly.

In order to check that the data are stationary, we compare the MSD obtained from the increments $\{x_t = X_{t+T} - X_T\}_{T \leq N/4, t}$ in the first quarter of the data and the increments $\{x_t = X_{t+T} - X_T\}_{3N/4 \leq T, t}$ in the last quarter of the data. Indeed, for all datasets the MSD in the two sub-intervals of the data have similar growth, i.e. the aging exponent is $\alpha = 0$. We note that for the river flow dataset there is difference a constant prefactor. This transient aging explains the small deviations in Fig. 3 (a') of the main text from the behavior of a stationary process characterized by the persistence exponent $\theta = 1 - 1/d_w$. However, since the walk dimension is not changed, $\alpha = 0$ and the record age exponent is still $1/d_w$ for this dataset.

Record ages are obtained by starting the subtrajectories at values of t equally spaced at intervals at least 200 time steps long, and observing successive records occurring in the subtrajectory. First return times are obtained by starting the subtrajectories at any value of time.



Supplementary Figure 6. **Characterization of the data used in Fig. 3 of the main text:**

(a) river discharge, (b) volcanic soil temperature, (c) motion of microspheres in a gel, (d) motion of vacuoles inside an amoeba, (e) motion of telomeres, (f) DNA RW, (g) cumulative air temperature, and (h) Ethernet cumulative requests.

Top subfigures (a)- (h) show $F(\ell)$ obtained via the DMA method. The linear fit on the log-log plot is represented by a black dashed line.

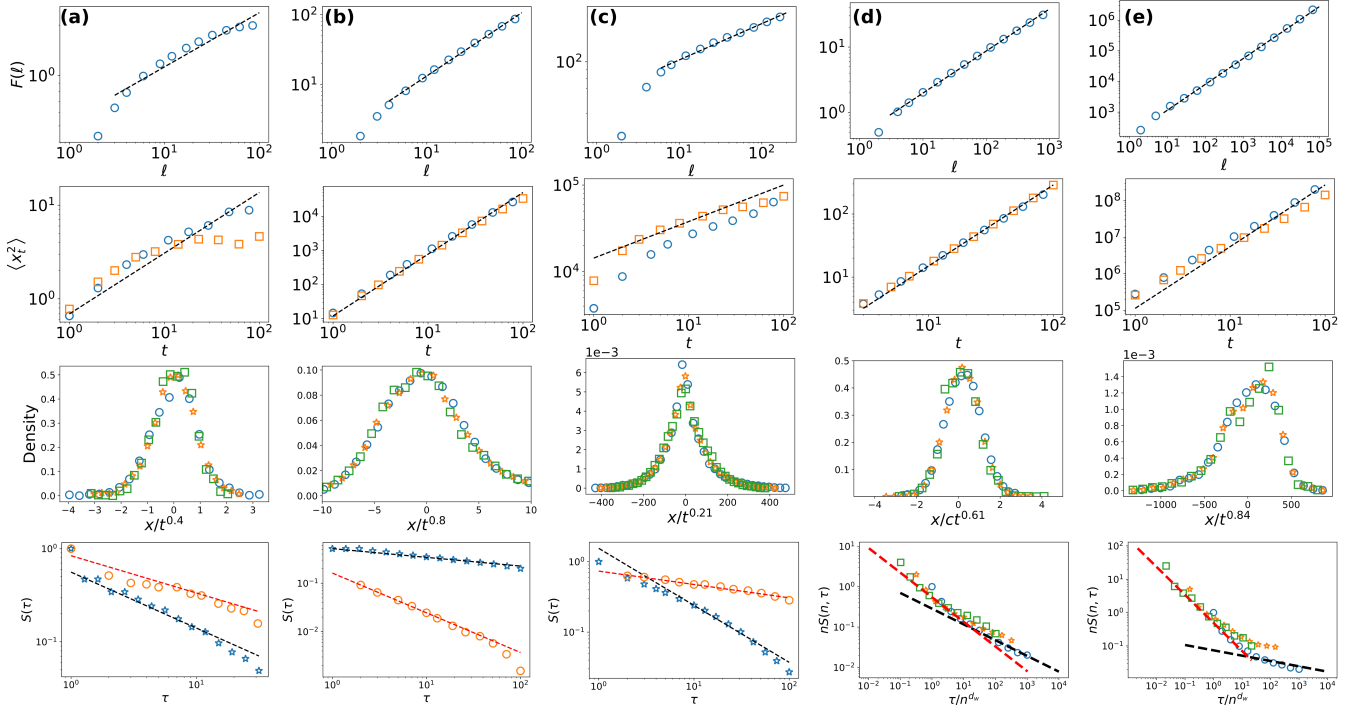
Bottom subfigures (a')- (h') show the MSD $\langle x_t^2 \rangle$ computed from the first (blue circles) and last (orange squares) quarters of the data. Black dashed line stands for the algebraic growth t^{2/d_w} where d_w was obtained via the DMA method.

C. Analysis of complementary datasets

We additionally conducted an analysis of the following complementary datasets to further demonstrate the broad applicability of our results:

- (a) *Volcanic soil temperature ($^{\circ}C$)*. Another dataset (measured at the Monte Sant'Angelo site) of soil temperatures monitored in the volcanic caldera of the Campi Flegrei area in Naples. It was shown in [S31, S32] that it is an fBm of parameter $H \approx 0.4$ once the data have been detrended by removing the linear trends between two temperature extrema (between two solstices). Here we also detrend the data by removing the same linear seasonal trends.
- (b) *Cumulative air temperature at Montélimar ($^{\circ}C.day$)*. As for the soil temperature in [S31], we remove the linear trends between two solstices. In this case, the temperature fluctuations are fractional Gaussian noise (fGn) and not fBm, in agreement to what was observed in [S37] for the data at London. We obtain a Hurst exponent $H \approx 0.8$ via the DMA method.
- (c) *Rhône river discharge (m^3/s)*. We consider the daily mean debit of the Rhône measured at the Sault Brenaz station [S40]. It was observed that this quantity presents correlations which can be modeled by subdiffusive non-Markovian RW [S28]. In this time series, we obtain $H \approx 0.21$ by applications of the DMA method.
- (d) *DNA RW*. We consider the human T-cell receptor α/δ sequence from the GenBank data base (HUMTCRADCV). It was observed in [S35, S36] that the process is a RW with long-range correlations of Hurst exponent $H \approx 0.61$. We estimate and remove the bias $\hat{v} = \frac{1}{N} \sum_{t=1}^N \eta_t$ in the data by replacing η_t by $\eta_t - \hat{v}$.
- (e) *Cumulative Ethernet traffic (10 bytes.ms)*. The dataset represents the number of packets going through an Ethernet cable every 10 ms at the Bellcore Morristown Research and Engineering facility [S38]. In particular, in [S39], it was shown that the process is a fGn of dimension $H \approx 0.84$. This is why we consider the cumulative number of requests up to a given time t . We detrend the cumulative data in the same manner as the DNA RW by removing the estimated bias \hat{v} at every step. We display the data measured in October 1989.

All considered complementary datasets support our theoretical results.



Supplementary Figure 7. **Analysis of record ages for non-Markovian RWs: theoretical predictions (lines) vs real time observations (symbols):** (a) volcanic soil temperature (Monte Sant'Angelo site), (b) cumulative air temperature (Montélimar), (c) river discharge (Rhône), (d) DNA RW (HUMTCRADCV), and (e) Ethernet cumulative requests (October 1989).

First line, $F(\ell)$ obtained via the DMA method and linear fit to the log-log representation shown by black dashed line.

Second line, check of the MSD $\langle x_t^2 \rangle$ computed from the first (blue circles) and last (orange squares) quarters of the data. Black dashed line shows linear fit to the log-log representation of the MSD data, given the same exponent $2/d_w$.

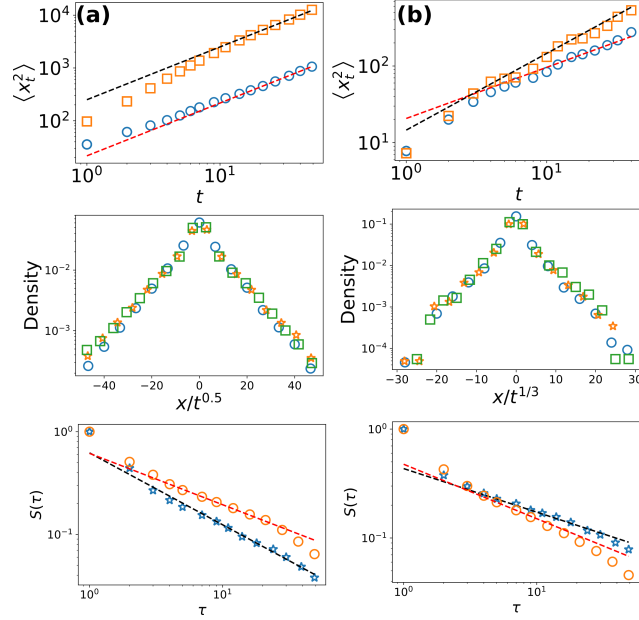
Third line, distribution of the increment $x_t = X_{t+T} - X_T$ at different times t normalised by t^{1/d_w} , where d_w was obtained via the DMA method for: (a) $t = 5, 10$ and 20 (b) $t = 5, 10$ and 20 (c) $t = 10, 20$ and 40 (d) $t = 20, 40$ and 80 (e) $t = 500, 1000$ and 2000 . Increasing values of times are represented successively by blue circles, orange stars and green squares.

Fourth line, (a)-(c) statistics of the time to first reach the initial value in the sub interval (blue stars) and the statistics of the records (regardless of the number n of records, orange circles) and (d)-(e) rescaled tail distribution of record ages τ_n for different values of the number of records n ($n = 1, 2$ and 4 for (d) and $n = 1, 5, 25$ for (e)). The black dashed line represents the algebraic decay $\tau^{-\theta}$ while the red dashed line stands for the algebraic decay τ^{-1/d_w} .

D. Datasets displaying aging of the increments

We also analysed the following complementary datasets which present aging in the increments:

- (a) *Single cell displacement on a 1d medium (half-pixels=0.65 μm).* We analyze the motion of MDCK (Madin-Darby Canine Kidney) epithelial cells on micro-contact-printed 1d linear tracks of fibronectin obtained in [S41], who found that the cells perform a Persistent Self-Attractive Walk (PSATW, which is a generalization of the SATW with a finite correlation length) motility behaviour, such that $d_w = d_w^0 = 2$. Because of the (transient, $\alpha = 0$) aging in the data, the persistence exponent θ is different from $1/2$.
- (b) *Single cell displacement on a 2d medium (pixels=1.3 μm).* We analyze the motion of MDCK epithelial cells on a 2d substrate obtained in [S41], who found that the cells show a PSATW motility behaviour, such that $d_w = 3$ and $d_w^0 = 2$ in agreement with theoretical and numerical observations for this type of model in 2d [S42, S43]. We consider that motion in x and y are i.i.d. and thus form two independent 1d trajectories. Because of the aging in the data, the persistence exponent θ is different from $1/2$.



Supplementary Figure 8. **Analysis of record ages for non-Markovian RWs: theoretical predictions (lines) vs experimental data displaying aging of the increments (symbols).** Cell motility on a (a) 1d and (b) 2d micropatterned surfaces.

First line, MSD $\langle x_t^2 \rangle$ computed at early times (blue circles, to compare with the red line $\propto t^{2/d_w}$) and at latter times (orange squares, to compare with the black line $\propto t^{2/d_w^0}$).

Second line, distribution of the increment $x_t = X_{t+T} - X_T$ at different times t normalised by t^{1/d_w} , where d_w was derived in [S41], for $t = 5, 10$ and 20 ($T < 50$). Increasing values of times are represented successively by blue circles, orange stars and green squares.

Third line, statistics of the time to first reach the initial value in the sub interval (blue stars) and the statistics of the records (regardless of the number n of records, orange circles). The black dashed line stands for the algebraic decay $\tau^{-\theta}$, where θ is estimated to be (a) $\theta \approx 0.7$ and (b) $\theta \approx 0.4$, and the red line represents the algebraic decay τ^{-1/d_w^0} .

Supplementary Figure 8 shows the analysis of datasets (a) and (b). Note that, because of aging, the persistence exponent $\theta \neq 1 - 1/d_w$. We conclude that these complex examples also support our theory.

SUPPLEMENTARY REFERENCES

- [S1] J. H. P. Schulz, E. Barkai, and R. Metzler, Aging renewal theory and application to random walks, *Phys. Rev. X* **4**, 011028 (2014).
- [S2] N. Levner, O. Bénichou, T. Guérin, and R. Voituriez, Universal first-passage statistics in aging media, *Phys. Rev. E* **98**, 022125 (2018).
- [S3] C. Godrèche and J.-M. Luck, Record statistics of integrated random walks and the random acceleration process, *J. Stat. Phys.* **186**, 4 (2022).
- [S4] J.-P. Bouchaud and A. Georges, Anomalous diffusion in disordered media: Statistical mechanisms, models and physical applications, *Phys. Rep.* **195**, 127–293 (1990).
- [S5] D. Carpentier and P. Le Doussal, Glass transition of a particle in a random potential, front selection in nonlinear renormalization group, and entropic phenomena in Liouville and sinh-Gordon models, *Phys. Rev. E* **63**, 026110 (2001).
- [S6] A. J. Bray, S. N. Majumdar, and G. Schehr, Persistence and first-passage properties in nonequilibrium systems, *Adv. Phys.* **62**, 225 (2013).
- [S7] J. Krug, H. Kallabis, S. Majumdar, S. Cornell, A. J. Bray, and C. Sire, Persistence exponents for fluctuating interfaces, *Phys. Rev. E* **56**, 2702 (1997).
- [S8] A. Hansen, T. Engøy, and K. J. Måløy, Measuring hurst exponents with the first return method, *Fractals* **2**, 527 (1994).
- [S9] M. Ding and W. Yang, Distribution of the first return time in fractional brownian motion and its application to the study of on-off intermittency, *Phys. Rev. E* **52**, 207 (1995).
- [S10] S. Maslov, M. Paczuski, and P. Bak, Avalanches and $\frac{1}{f}$ noise in evolution and growth models, *Phys. Rev. Lett.* **73**, 2162 (1994).
- [S11] C. S. Ryu and I.-m. Kim, Solid-on-solid model with next-nearest-neighbor interaction for epitaxial growth, *Phys. Rev. E* **52**, 2424 (1995).
- [S12] A. Barbier-Chebbah, O. Benichou, and R. Voituriez, Anomalous persistence exponents for normal yet aging diffusion, *Phys. Rev. E* **102**, 062115 (2020).
- [S13] V. B. Sapozhnikov, Self-attracting walk with $\nu < 1/2$, *J. Phys. A: Math. Gen.* **27**, L151 (1994).
- [S14] B. Davis, Reinforced random walk, *Probab. Theor. Rel. Fields* **84**, 203–229 (1990).
- [S15] A. Barbier-Chebbah, O. Bénichou, and R. Voituriez, Self-interacting random walks: Aging, exploration, and first-passage times, *Phys. Rev. X* **12**, 011052 (2022).
- [S16] H. C. Ottinger, The generalised true self-avoiding walk—a model with continuously variable exponent ν , *J. Phys. A: Math. Gen.* **18**, L363 (1985).
- [S17] D. J. Amit, G. Parisi, and L. Peliti, Asymptotic behavior of the “true” self-avoiding walk, *Phys. Rev. B* **27**, 1635 (1983).
- [S18] L. Pietronero, Critical dimensionality and exponent of the “true” self-avoiding walk, *Phys. Rev. B* **27**, 5887 (1983).
- [S19] S. P. Obukhov and L. Peliti, Renormalisation of the ‘true’ self-avoiding walk, *J. Phys. A: Math. Gen.* **16**, L147 (1983).
- [S20] B. Toth, The “True” Self-Avoiding Walk with Bond Repulsion on \mathbb{Z} : Limit Theorems, *Ann. Probab.* **23**, 1523 (1995).
- [S21] M. Radice, M. Onofri, R. Artuso, and G. Cristadoro, Transport properties and ageing for the averaged lévy–lorentz gas, *J. Phys. A: Math. Theor.* **53**, 025701 (2019).
- [S22] M. Radice, M. Onofri, R. Artuso, and G. Pozzoli, Statistics of occupation times and connection to local properties of nonhomogeneous random walks, *Phys. Rev. E* **101**, 042103 (2020).
- [S23] H. Safdari, A. V. Chechkin, G. R. Jafari, and R. Metzler, Aging scaled brownian motion, *Phys. Rev. E* **91**, 042107 (2015).
- [S24] S. C. Lim and S. V. Muniandy, Self-similar gaussian processes for modeling anomalous diffusion, *Phys. Rev. E* **66**, 021114 (2002).
- [S25] J.-H. Jeon, A. V. Chechkin, and R. Metzler, Scaled brownian motion: a paradoxical process with a time dependent diffusivity for the description of anomalous diffusion, *Phys. Chem. Chem. Phys.* **16**, 15811 (2014).
- [S26] Y. He, S. Burov, R. Metzler, and E. Barkai, Random time-scale invariant diffusion and transport coefficients, *Phys. Rev. Lett.* **101**, 058101 (2008).
- [S27] GRDC, Dresden mean daily discharge (1920-1992), data from the Global Runoff Data Centre (GRDC), <https://portal.grdc.bafg.de/applications/>.
- [S28] Q. Zhang, C.-Y. Xu, Y. D. Chen, and Z. Yu, Multifractal detrended fluctuation analysis of streamflow series of the Yangtze river basin, China, *Hydrol. Process.* **22**, 4997 (2008).
- [S29] M. Höll, K. Kiyono, and H. Kantz, Theoretical foundation of detrending methods for fluctuation analysis such as detrended fluctuation analysis and detrending moving average, *Phys. Rev. E* **99**, 033305 (2019).
- [S30] E. Alessio, A. Carbone, G. Castelli, and V. Frappietro, Second-order moving average and scaling of stochastic time series, *Eur. Phys. J. B* **27**, 197 (2002).
- [S31] A. Di Crescenzo, B. Martinucci, and V. Mustaro, A model based on fractional brownian motion for temperature fluctuation in the Campi Flegrei caldera, *Fractal Fract.* **6**, 421 (2022).
- [S32] C. Sabbarese, F. Ambrosino, G. Chiodini, F. Giudicepietro, G. Macedonio, S. Caliro, W. De Cesare, F. Bianco, M. Pugliese, and V. Roca, Continuous radon monitoring during seven years of volcanic unrest at Campi Flegrei caldera (Italy), *Sci. Rep.* **10**, 9551 (2020).
- [S33] D. Krapf, N. Lukat, E. Marinari, R. Metzler, G. Oshanin, C. Selhuber-Unkel, A. Squarcini, L. Stadler, M. Weiss, and X. Xu, Spectral content of a single non-brownian trajectory, *Phys. Rev. X* **9**, 011019 (2019).
- [S34] L. Stadler and M. Weiss, Non-equilibrium forces drive the anomalous diffusion of telomeres in the nucleus of mammalian cells, *New J. Phys.* **19**, 113048 (2017).

- [S35] C.-K. Peng, S. V. Buldyrev, S. Havlin, M. Simons, H. E. Stanley, and A. L. Goldberger, Mosaic organization of dna nucleotides, *Phys. Rev. E* **49**, 1685 (1994).
- [S36] C.-K. Peng, S. V. Buldyrev, A. L. Goldberger, S. Havlin, F. Sciortino, M. Simons, and H. E. Stanley, Long-range correlations in nucleotide sequences, *Nature* **356**, 168 (1992).
- [S37] D. C. Brody, J. Syroka, and M. Zervos, Dynamical pricing of weather derivatives, *Quant. Finance* **2**, 189 (2002).
- [S38] H. Fowler and W. Leland, Local area network characteristics, with implications for broadband network congestion management, *IEEE J. Sel. Areas Commun.* **9**, 1139 (1991).
- [S39] W. E. Leland, M. S. Taqqu, W. Willinger, and D. V. Wilson, On the self-similar nature of ethernet traffic, in *Conference proceedings on Communications architectures, protocols and applications* (1993) pp. 183–193.
- [S40] GRDC, Rhône mean daily discharge at the sault brenaz station (1920-1992), data from the Global Runoff Data Centre (GRDC), <https://portal.grdc.bafg.de/applications/>.
- [S41] J. d’Alessandro, A. Barbier-Chebbah, V. Cellerin, O. Benichou, R. M. Mège, R. Voituriez, and B. Ladoux, Cell migration guided by long-lived spatial memory, *Nat. Commun.* **12**, 4118 (2021).
- [S42] A. Ordemann, E. Tomer, G. Berkolaiko, S. Havlin, and A. Bunde, Structural properties of self-attracting walks, *Phys. Rev. E* **64**, 046117 (2001).
- [S43] J. G. Foster, P. Grassberger, and M. Paczuski, Reinforced walks in two and three dimensions, *New J. Phys.* **11**, 023009 (2009).